ADVANCED HEALTHCARE MATERIALS
www.advhealthmat.de

Graphene Oxide-Doped Gellan Gum–PEGDA Bilayered Hydrogel Mimicking the Mechanical and Lubrication Properties of Articular Cartilage

Diego Trucco, Lorenzo Vannozzi, Eti Teblum, Madina Telkhozhayeva, Gilbert Daniel Nessim, Saverio Affatato, Hind Al-Haddad, Gina Lisignoli,* and Leonardo Ricotti**

Articular cartilage (AC) is a specialized connective tissue able to provide a low-friction gliding surface supporting shock-absorption, reducing stresses, and guaranteeing wear-resistance thanks to its structure and mechanical and lubrication properties. Being an avascular tissue, AC has a limited ability to heal defects. Nowadays, conventional strategies show several limitations, which results in ineffective restoration of chondral defects. Several tissue engineering approaches have been proposed to restore the AC's native properties without reproducing its mechanical and lubrication properties yet. This work reports the fabrication of a bilayered structure made of gellan gum (GG) and poly (ethylene glycol) diacrylate (PEGDA), able to mimic the mechanical and lubrication features of both AC superficial and deep zones. Through appropriate combinations of GG and PEGDA, cartilage Young's modulus is effectively mimicked for both zones. Graphene oxide is used as a dopant agent for the superficial hydrogel layer, demonstrating a lower friction than the nondoped counterpart. The bilayered hydrogel's antiwear properties are confirmed by using a knee simulator, following ISO 14243. Finally, in vitro tests with human chondrocytes confirm the absence of cytotoxicity effects. The results shown in this paper open the way to a multilayered synthetic injectable or surgically implantable filler for restoring AC defects.

1. Introduction

Cartilage is a specialized avascular and aneural connective tissue capable of bearing mechanical stresses without permanent distortion. Three types of cartilage tissue (elastic, fibrocartilage, and hyaline) are distributed in different parts of the human body, designated to perform specific functions depending on their structural composition.[1] In particular, hyaline cartilage, also named articular cartilage (AC), is the most common type of cartilage that is present in hips, elbows, shoulders, and knee joints. It covers the opposing bone surfaces within each joint, providing a low-friction gliding surface for the articulation supporting shock-absorption, distributing loads, reducing stresses on the subchondral bone, and guaranteeing wear resistance.[2]

AC is an anisotropic and viscoelastic tissue. From a functional and structural viewpoint, it can be divided into four zones (superficial, middle, deep, calcified), which vary in extracellular matrix (ECM) composition, density, collagen fibers assembling, phenotype, and chondrocyte activity.[2b,3] Overall, the AC can be considered divided in two macroregions: a superficial and a deep one. The superficial zone provides the smooth gliding surface guaranteeing lubrication and low wear of the joint, exhibiting a lower tensile strength and stiffness than the deeper zones in terms of compressive properties.[2b] The deep zone represents the bridge

D. Trucco, Dr. L. Vannozzi, H. Al-Haddad, Prof. L. Ricotti
The BioRobotics Institute
Scuola Superiore Sant'Anna
Piazza Martiri della Libertà 33, Pisa 56127, Italy
E-mail: diego.trucco@santannapisa.it; leonardo.ricotti@santannapisa.it

D. Trucco, Dr. L. Vannozzi, H. Al-Haddad, Prof. L. Ricotti
Department of Excellence in Robotics & AI
Scuola Superiore Sant'Anna
Piazza Martiri della Libertà 33 Pisa 56127, Italy

The ORCID identification number(s) for the author(s) of this article can be found under https://doi.org/10.1002/adhm.202001434

DOI: 10.1002/adhm.202001434

D. Trucco, Dr. G. Lisignoli
IRCSS Istituto Ortopedico Rizzoli
SC Laboratorio di Immunoreumatologia e Rigenerazione Tissutale
Via di Barbiano, 1/10 Bologna 40136, Italy
E-mail: gina.lisignoli@ior.it

Dr. E. Teblum, M. Telkhozhayeva, Prof. G. D. Nessim
Department of Chemistry
Bar-Ilan University
Ramat Gan 52900, Israel

Dr. E. Teblum, M. Telkhozhayeva, Prof. G. D. Nessim
Bar Ilan Institute for Nanotechnology and Advanced Materials (BINA)
Bar-Ilan University
Ramat Gan 52900, Israel

Dr. S. Affatato
IRCSS Istituto Ortopedico Rizzoli
Laboratorio Tecnologie Biomediche
Via di Barbiano, 1/10 Bologna 40136, Italy

between cartilage and bone and provides the highest resistance to compressive forces during the movement of the joint.

The mechanical properties of AC differ from layer to layer.[4] In particular, the compression Young's modulus is in the range of 280 ± 160 to 730 ± 260 kPa for the superficial and deep regions, respectively. This is mainly due to their different permeability to the synovial fluid flow.[5] Overall, compression tests performed on the human knee AC exhibited a full-thickness compression Young's modulus of 581 ± 168 kPa.[4,5b,6]

Lubrication is another crucial property of AC. The superficial zone of AC provides a low-friction gliding surface for the synovial joint, due to an extremely low coefficient of friction between cartilage and cartilage (0.001–0.03).[5b] However, damages to the superficial area may lead to a rapid wearing of AC and subsequent cartilage breakdown.[3b]

AC damages constitute the most common injuries of the knee joints.[7] At the origin of the damage, there are mechanical injuries (i.e., adventitious or sport-related traumas)[8] or age-related degeneration (i.e., osteoarthritis (OA)). However, also risk factors such as obesity and genetic predisposition increase the probability to incur in a progressive AC degeneration.[9] Two types of defects can mainly occur: chondral (partial and full thickness) and osteochondral defects.[8a,10] Chondral defects only affect AC and do not extend to the underlying subchondral bone, while osteochondral lesions involve both cartilage and the subchondral bone.[11] In osteochondral injuries, blood cells and mesenchymal progenitor cells have access to the damaged cartilage from the subchondral bone, and the healing process leads to the formation of weaker fibrous cartilage.[8c] Differently, chondral defects cannot self-regenerate at all. Conventional strategies, such as auto-, allo-, and xenografts or joint replacement full implants, have been adopted for cartilage repair, showing several limitations:[12] osteochondral autografts suffers from limited availability and risk of donor site morbidity;[13] osteochondral allografts are affected by low supply, short shelf-life and the need to find a fresh postmortem tissue from a very young donor;[13b] osteochondral xenografts might show an immunogenic response;[14] prostheses, necessary in case of irreparable AC damage, must be implanted via invasive surgery and the post-intervention recovery is long and complicated.

Tissue engineering (TE) approaches have evolved to restore damaged native tissues by targeting the development of tissue substitutes in vitro.[15] Scaffolds with a precise microarchitecture can support cell growth and the production of new ECM and, in the meantime, degrade to let the formation of the targeted biological tissue.[16] However, many TE approaches exhibit limitations in terms of clinical translation; in particular, it is difficult to reproduce the mechanical properties of the hyaline cartilage in vitro and, at the same time, to provide the scaffold with appropriate lubrication properties and let the scaffold degrade overtime without affecting such properties.[17]

Multilayer structures have been developed to regenerate osteochondral defects, which were composed of subchondral and cartilage zones.[18] Osteochondral structures typically show poor mechanical properties and low cell differentiation in the bone and chondral direction. It is not straightforward, with TE approaches, to reconstitute a multilayer structure featured by mechanical properties reflecting the ones of the natural cartilage.[19] Furthermore, TE constructs have to deal with a complex regulatory pathway before entering the clinics, being advanced therapy medicinal products bearing human cells. Fully synthetic (acellular) materials have the advantage of a simpler certification pathway, in addition to the fact that mechanical properties can be varied with higher flexibility, since cells are not embedded in the material and there is no need to keep them alive through a highly porous and soft environment.

Thus, synthetic acellular biomaterials can represent a valid alternative for the reparation of cartilage defects and the restoration of tissue functionalities and anatomical structures.[15a] The achievement of multilayered structures mimicking the zone-specific mechanical and lubrication properties of the AC would be highly promising for AC repair.[20] This approach can be used to produce a kind of hemiarthroplasty, such as common metal substitutes, that could reconstitute in situ the AC surface and also its overall mechanical properties.

Hydrogels are water-swollen materials that can be considered optimal candidates for being injected or placed in the joint and to form 3D structures in situ.[21] In the state-of-the-art, some materials such as poly(ethylene oxide terephthalate)/poly(butylene terephthalate) (PEOT/PBT),[22] poly(ϵ-caprolactone) (PCL),[23] collagen,[24] chondroitin sulphate (CS) and gelatin (G) microribbon (μRB),[19] have been shaped in multilayers and proposed as possible synthetic grafts for AC repair. However, none of them effectively mimicked both the mechanical and lubrication properties of native cartilage. Thus, further efforts are needed in this field.

Gellan gum (GG) is a water-soluble anionic polysaccharide produced by the bacterium *Sphingomonas elodea*.[25] GG has been widely studied in the TE field because of its properties such as biocompatibility, biodegradability, and ductility. In particular, its use has been particularly advantageous for the cartilage TE field because of its structural similarity with native AC glycosaminoglycans due to the presence of glucuronic acid residues in its repeating unit.[18c,26] This material is thermosensitive and can be ionically crosslinked, interacting with monovalent and divalent ions.[26a,27] GG has many advantages over other hydrogels, including shear-thinning properties and gel formation at physiological temperatures, which make it a qualified candidate for being injected into cartilage defects. However, the mechanical properties of such a hydrogel are far from those related to the target cartilage zones.[28]

In this paper, we explored the addition of poly (ethylene glycol) diacrylate (PEGDA) to improve both stiffness and toughness of GG. PEGDA is a synthetic polymer used as a prepolymer solution for the formation of a crosslinked polymeric network upon light exposure and the presence of a photoinitiator.[29] The combination of GG and PEGDA permits playing with both noncovalent and covalent crosslinking methods, to achieve an interpenetrated polymeric network able to effectively recover its shape after loading, as well as to show adequate compressive strength. As mentioned, the achievement of optimal lubrication properties is also a significant challenge, which is needed to improve the performance of the cartilage substitutes. Carbon-based nanomaterials have been used in the literature to improve the mechanical and electrical properties of bare materials. Recently, graphene oxide (GO) has been claimed as an ideal nanomaterial for cartilage TE due to its chondroinductive properties when embedded into polymeric formulations.

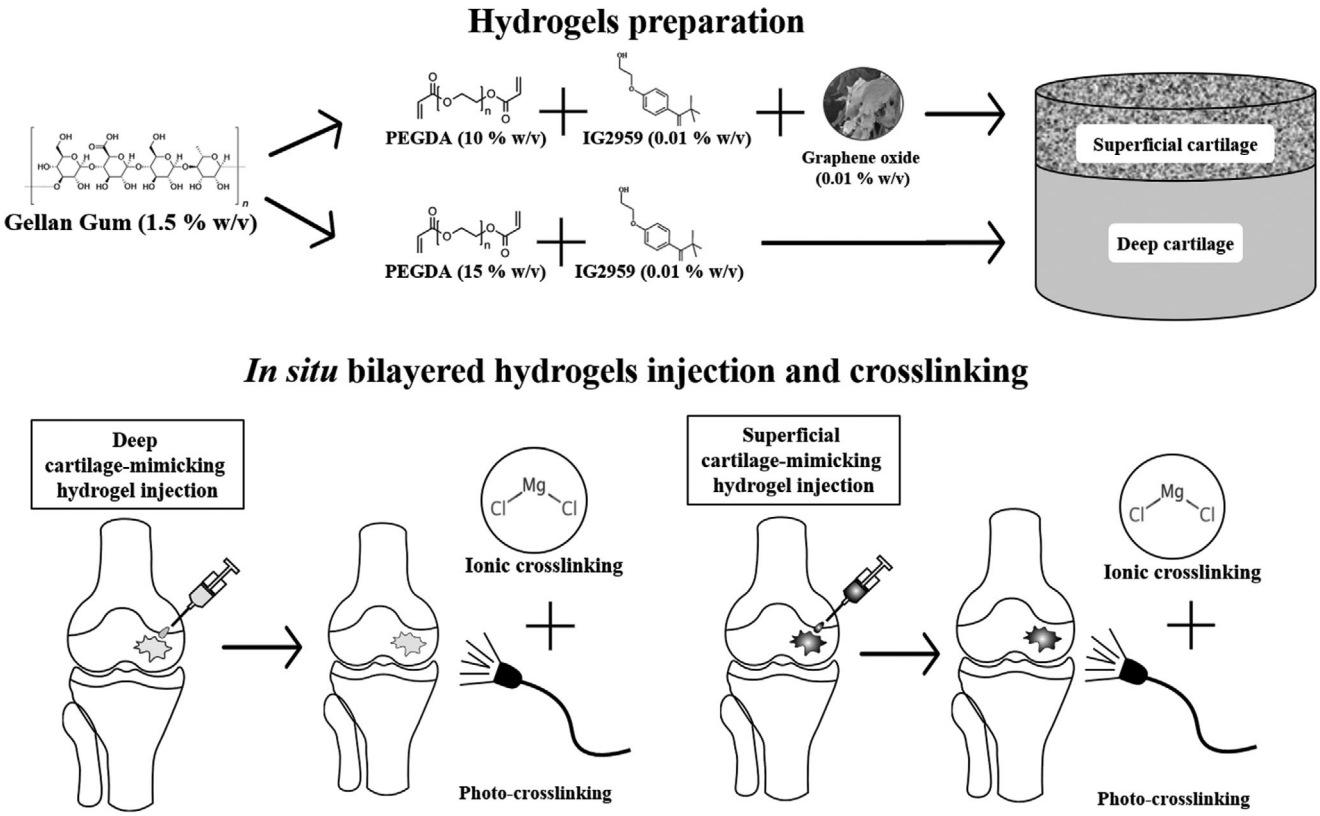

Figure 1. Depiction of the concept targeted in this work. By combining GG, PEGDA and GO, two hydrogels with specific properties, mimicking the ones of superficial and deep cartilage, respectively, are formulated. Then, the superficial and deep cartilage-mimicking hydrogels could be injected in situ and sequentially crosslinked using UV light (photo-crosslinking) and $CaCl_2$ solution (ionic crosslinking).

In fact, GO can provide a cell-friendly microenvironment able to enhance chondrogenic differentiation.[30] On the other hand, GO exhibits peculiar self-lubricating and anti-wear properties,[31] thanks to a high surface-to-volume ratio, a low effective threshold resulting from its nanometer dimensions, which leads to optimizing the performance of polymer composites.[32]

We hypothesize that, by combining GG, PEGDA and GO, we could be able to develop a bilayered hydrogel well mimicking both the mechanical features and the lubrication properties of native AC. Such a nanocomposite hydrogel could be used as an injectable filler or a surgically implantable substitute in chondral defects (**Figure 1** showing no cytotoxicity and guaranteeing suitable resistance to wear.

2. Results and Discussion

2.1. Mechanical Properties and Swelling Ratio

All combinations of GG and PEGDA at different concentrations and crosslinking approaches presented in the following are summarized in Table S1 (Supporting Information). **Figure 2** reports the results of the mechanical characterization of hydrogels combining GG and PEGDA at different concentrations, aimed at mimicking the superficial and deep cartilage. Data show a relevant increase in the Young's modulus when PEGDA concentration increased from 10 (GG/PEGDA10) to 15 (GG/PEGDA15) % w/v. This range of values was then compared with the mechanical properties of superficial and deep cartilage, featured by a Young's modulus of 280 ± 160 and 730 ± 260 kPa, respectively.[5b] The first layer included the superficial and the middle zones areas of a healthy cartilage, whereas the second layer included the deep zone of a healthy cartilage.

The effects of UV exposure time and ionic crosslinking with $MgCl_2$ were analyzed for each PEGDA concentration. The Young's modulus of GG/PEGDA10 hydrogels photocrosslinked for 5 min using a UV light source emitting at 365 nm at an intensity of 40 mW cm^{-2}, was significantly improved by ionic crosslinking from an average value of 122 ± 16 kPa (without ionic crosslinking, GG/PEGDA10_5 minUV) to 182 ± 65 kPa (with ionic crosslinking GG/PEGDA10_5 minUV_10 min$MgCl_2$) (* $p < 0.05$). Differently, no statistical difference was found between hydrogels photocrosslinked for 10 min at the same conditions of wavelength and intensity described above (without ionic crosslinking, GG/PEGDA10_10 minUV), showing a Young's modulus of 139 ± 33 kPa, and hydrogels similar, but subjected to ionic crosslinking (with ionic crosslinking GG/PEGDA10_10 minUV_10 min$MgCl_2$), resulting in a modulus of 166 ± 42 kPa. On the other hand, the Young's modulus of GG/PEGDA15 hydrogels photocrosslinked for 5 min (same conditions as before) improved from an average value of 738 ± 142 kPa (without ionic crosslinking, GG/PEGDA15_5 minUV) to 801 ± 152 kPa (with

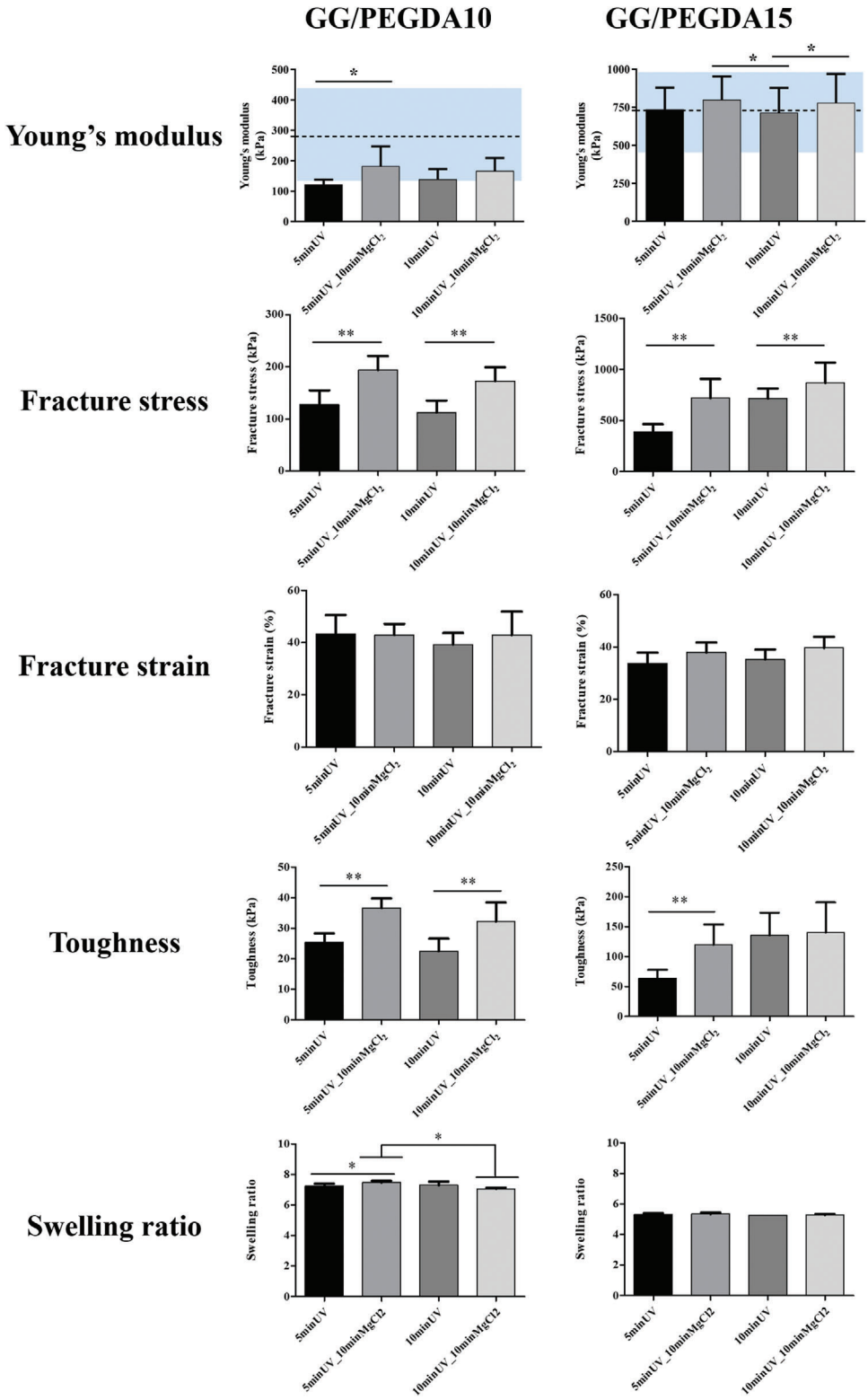

Figure 2. Mechanical characterization of GG/PEGDA10 and GG/PEGDA15 hydrogels, in terms of: Young's modulus, fracture stress, fracture strain, toughness and swelling ratio. For the Young's modulus, the blue areas represent the range of stiffness reported in O'Connell et al.[5b] for the native articular cartilage. Data presented as mean ± SD, $n = 5$, p-values are calculated using the one-way ANOVA with Tukey's post-test correction, * $p < 0.05$, ** $p < 0.01$. Analyzed samples: GG/PEGDA10_5 minUV, GG/PEGDA10_5 minUV_10 minMgCl$_2$, GG/PEGDA10_10 minUV, GG/PEGDA10_10 minUV_10 minMgCl$_2$, GG/PEGDA15_5 minUV, GG/PEGDA15_5 minUV_10 minMgCl$_2$, GG/PEGDA15_10 minUV, GG/PEGDA15_10 minUV_10 minMgCl$_2$.

ionic crosslinking, GG/PEGDA15_5 minUV_10 min$MgCl_2$), but without any statistical difference. Finally, increasing the time of photopolymerization to 10 min, a statistically significant difference (*$p < 0.05$) in the Young's modulus was found, between absence (715 ± 163 kPa, GG/PEGDA15_10 minUV) and presence (780 ± 190 kPa, GG/PEGDA15_10 minUV_10 min$MgCl_2$) of ionic crosslinking.

These results, together with the ones shown in Figure S1 (Supporting Information), demonstrate that the PEGDA concentration can modulate the rather low mechanical properties of GG, in agreement with other reports.[33] Indeed, the properties of PEGDA can be varied by acting on its molecular weight, concentration, photoinitiator concentration and crosslinking parameters such as exposure time.[34] The scientific literature also confirms the relevant role of ionic-crosslinking in the improvement of hydrogels Young's moduli.[35] Only one study focused on analyzing the blend of GG and PEGDA (Mn: 6000), even if its primary purpose was the evaluation of the blend printability. In this study, 1.5% GG blended with 10% PEGDA was analyzed and a comparison between the Young's moduli of this material in different conditions (non-crosslinked, photo-crosslinked and, double (photo- and ionic) was made. The Young's modulus evaluated through compression tests was improved from 40 to 60 kPa and to 184 kPa, respectively, for the above-mentioned crosslinking conditions.[35] In our case, the combination between GG and PEGDA and the possibility to increase the UV exposure time and PEGDA concentration allowed achieving values closer to the ones featuring the different zones of the human AC, namely 280 ± 160 kPa (superficial) and 730 ± 260 kPa (deep), evidenced with blue regions in the graphs of Figure 2 which constitutes an original result, for this material.

The adoption of a dual crosslinking strategy (optical and chemical one) also allowed to modulate other important mechanical features of the hydrogels. The fracture stress of GG/PEGDA10 hydrogels photo-crosslinked for 5 min was significantly improved from 127 ± 27 kPa (without ionic crosslinking, GG/PEGDA10_5 minUV) to 194 ± 27 kPa (with ionic crosslinking, GG/PEGDA10_5 minUV_10 min$MgCl_2$) (** $p < 0.01$). Similarly, the fracture stress for hydrogels photocrosslinked for 10 min was significantly improved from 112 ± 23 kPa (GG/PEGDA10_10 minUV) to 173 ± 26 kPa using the ionic crosslinking (GG/PEGDA10_10 minUV_10 min$MgCl_2$) (** $p < 0.01$). The same behavior was found in GG/PEGDA15 hydrogels in which the ionic crosslinking significantly improved the fracture stress of photo-crosslinked materials (** $p < 0.01$). Interestingly, the fracture strain of both GG/PEGDA10 and GG/PEGDA15 hydrogel formulations did not show any significant difference between the groups, ranging from values slightly larger than 40% for the hydrogels mimicking the superficial cartilage and slightly smaller than 40% for the hydrogels mimicking the deep cartilage. Such values can be considered suitable for the application in the cartilage TE field, being superior to the ones possessed by the native AC.[4]

Moreover, the toughness of both GG/PEGDA10 and GG/PEGDA15 hydrogels resulted statistically different between samples treated with or without ionic crosslinking (** $p < 0.01$). The toughness of GG/PEGDA10 was improved of around 1.5 fold when ionic crosslinking was applied for both photopolymerization times, whereas the toughness of GG/PEGDA15 hydrogels was improved significantly from 64 ± 14 kPa (GG/PEGDA15_5 minUV) to 119 ± 34 kPa (GG/PEGDA15_5 minUV_10 min$MgCl_2$) (5 min of photopolymerization) (** $p < 0.01$). The toughness values of GG/PEGDA15_10 minUV and GG/PEGDA15_10 minUV_10 min$MgCl_2$ (10 min photopolymerization) were not significantly different, being 136 ± 34 and 140 ± 50 kPa, respectively.

The hydrogel formulations described above showed interesting mechanical properties, which had not been deeply investigated, so far, in the state-of-the-art concerning this material type. Interestingly, the results highlighted that ionic crosslinking with $MgCl_2$ in addition to DMEM led to a statistically significant improvement of the Young's modulus, fracture stress, and toughness. Besides, 5 min of UV exposure for each layer allowed keeping the crosslinking time lower while maintaining an optimal polymerization degree. The contribution of ionic crosslinking proved more effective than the UV exposure time. In fact, an overall increase in the mechanical properties of the hydrogels was observed, when comparing the samples crosslinked with the same UV light timing but with the additional ionic crosslinking with $MgCl_2$. This enhancement is probably due to an increase in the number of divalent cations (Mg^{2+}) that promoted the aggregation of GG chains and formed a more robust polymer network structure. Among the candidate divalent cations, $MgCl_2$ was chosen because it proved to have a positive effect on cartilage tissues affected by degenerative diseases, like osteoarthritis.[36]

Several blend compositions with various mechanical properties have been developed in the cartilage TE field, so far. Strontium alginate (Alg-Sr) and strontium alginate/chondroitin sulfate (Alg/CS-Sr) hydrogels have been proposed as interesting blends with tunable mechanical properties for cartilage TE. Both blends showed intriguing biological features, but their compression Young's moduli were far from the target values featuring the natural AC (less than 60 kPa for Alg-Sr and less than 120 kPa for Alg/CS-Sr).[37] Another study focused on the development of an interpenetrating hydrogel made of agar and polyacrylamide (PAAm), which were physically and ionically crosslinked. The resulting hydrogels exhibited a linear stiffness that improved by increasing the Agar concentration up to 313 kPa (30 mg mL^{-1}), a value which is far from the desired one (581 ± 168 kPa[4,5b,6]), if full-thickness cartilage tissue substitution is targeted.[38] Fully synthetic hydrogels, composed of poly (2-acrylamido-2-methylpropanesulfonic acid) (PAMPS) and poly (*N*-isopropylacrylamide-*co*-acrylamide) [P(NIPAAm-*co*-AAm)], were also evaluated as potential off-the-shelf materials for cartilage replacement.[39] These hydrogels have been developed without reproducing cartilage-specific zones and achieving 1 MPa as a target Young's modulus: this value could be too high for human cartilage tissue substitution. Moreover, these hydrogels were hard to be developed in situ due to reactions that typically produce toxic compounds.

In addition to the mechanical analyses, the swelling ratio of the different samples was calculated, to get hints on the crosslinking density of each material formulation and to verify if there were any significant changes due to different concentrations and/or different crosslinking parameters. Figure 2 also shows that the different crosslinking parameters, while keeping the same PEGDA concentration, did not significantly modify the swelling

degree. On the other hand, different PEGDA concentrations produced different swelling ratios. This indicates a higher crosslinking density for GG/PEGDA15 hydrogels, as also confirmed by mechanical properties. Based on the results obtained, we chose the best candidates (GG/PEGDA10_5 minUV_10 min$MgCl_2$ and GG/PEGDA15_5 minUV_10 min$MgCl_2$), namely the ones showing mechanical properties as close as possible to the ones of the superficial and deep zones of the AC.[7b]

2.2. Hydrogel Doped with Graphene Oxide

GO which is known for its remarkable mechanical and lubrication properties, was selected for doping the GG/PEGDA10_5 minUV_10 min$MgCl_2$ hydrogel (the one mimicking the superficial AC zone). Previous studies showed that GG is a suitable reducing agent for stabilizing the dispersion of nanofillers in aqueous solutions.[40] However, only a few studies have explored the combination of GG and carbon-based dopants to improve the mechanical properties of these hydrogels.[41]

GO was synthesized using the modified Hummer's method.[42] **Figure 3**a,b shows SEM images and Raman spectrum (with a laser wavelength of 532 nm) of the layered GO bulk. Raman analysis confirmed the two characteristic bands at 1360 cm^{-1} (D band) and 1606 cm^{-1} (G band) related to GO. After sonication of the GO in ethanol, a droplet from the dispersion was drop casted on a Si/SiO_2 wafer and let dry overnight; this allowed to observe flakes with a minimum average thickness of 4.0 ± 0.3 nm which was measured using atomic force microscopy (AFM; Figure 3c. Additionally, we performed high-resolution transmission electron microscopy (HRTEM) to confirm the layered structure of GO at the nanoscale (Figure 3d).

GO (0.01% w/v) was added, as mentioned, to the GG/PEGDA10_5 minUV_10 min$MgCl_2$ hydrogel formulation, obtaining a homogeneous dispersion of the nanomaterial in the matrix (Figure S2, Supporting Information). This was facilitated by the low concentration used (0.01% w/v), which also minimizes the cytotoxicity risk of GO, which is known to be dose-dependent.[43] With the concentration used in this paper, previous reports highlighted an increased mesenchymal stem cell (MSCs) growth with respect to the controls, thus resulting beneficial, rather than toxic.[44]

The mechanical properties of GG/PEGDA10_5 minUV_10 min$MgCl_2$ and the corresponding GO-doped hydrogel (GG/PEGDA10/GO_5 minUV_10 min$MgCl_2$) were compared in order to assess the role of GO in modulating the behavior of samples photo-crosslinked for 5 min and subsequently ionically crosslinked with $MgCl_2$ (Figure 3e). The use of such a concentration of GO led to a slight increase (not statistically significant) in the hydrogel stiffness (from 182 ± 26 to 248 ± 21 kPa). However, the stiffness of the nanocomposite was still included in the range featuring the native human superficial cartilage zone.[5b] The fracture strain did not change with the addition of the nanofiller. On the other hand, the average value of fracture stress and toughness increased significantly, from 194 ± 27 to 246 ± 34 kPa and from 36 ± 3 to 41 ± 9 kPa, respectively. The toughness of the GO-doped hydrogel showed an improvement, probably due to the higher energy dissipation in the presence of GO nanosheets, highlighting a better mechanical performance than the bare hydrogel.[45] As well, fracture stress increased thanks to the dopant agent, which acted as a reinforcement agent of synthetic cartilage tissue. These results are in line with other pieces of evidence available in the scientific literature.[46] For example, in poly(vinyl alcohol) (PVA)/GO nanocomposite hydrogels, a significant reinforcement was ascribed to the formation of a dense and stable crosslinking network at different concentrations of the polymer due to the presence of micron-sized GO (≈0.3% w/v). In our case, the introduction of a relatively low concentration of GO (0.01% w/v) did not lead to a statistical difference with the bare hydrogel in term of Young's modulus, thus allowing to remain in the range of the target value for mimicking the superficial AC tissue. Nevertheless, other crucial mechanical properties, such as fracture stress and toughness, were significantly improved, thus highlighting that even a low concentration of GO can guarantee important reinforcing mechanisms.[47] Moreover, we observed that the swelling ratio slightly decreased by adding the GO nanofiller (from 7.2 ± 0.2 to 6.5 ± 0.3), but without any statistical significance.

Lubrication tests were performed on the superficial cartilage-mimicking samples (GG/PEGDA10_5 minUV_10 min$MgCl_2$ and GG/PEGDA10/GO_5 minUV_10 min$MgCl_2$) in order to assess if the presence of the GO nanosheets could improve lubrication properties. A depiction of the set-up for the evaluation of the lubrication properties is shown in **Figure 4**a. The lubrication test to determine the coefficient of friction (COF) was divided into two intervals, according to the Stribeck curve, which provides information on the different friction regimes.[48]

As shown in Figure 4b, the COF gradually grew in the static regime for both GG/PEGDA10_5 minUV_10 min$MgCl_2$ and GG/PEGDA10/GO_5 minUV_10 min$MgCl_2$ hydrogels for both lubricants until transition to kinematic regime. Then, the COF of all conditions maintained a constant trend in the kinetic regime for rotational speeds up to 0.5 min^{-1}. After this point, the COF values increased due to the higher speed of testing. As shown in Figure 4b, both nondoped and GO-doped hydrogels lubricated with either PBS and synthetic synovial fluid showed COF values comparable with the ones of natural articular cartilage, up to the transition area between the static and dynamic regions.[5b] Indeed, the COF of GG/PEGDA10_5 minUV_10 min$MgCl_2$ and GG/PEGDA10/GO_5 minUV_10 min$MgCl_2$ in presence of PBS was 0.022 ± 0.004 and 0.013 ± 0.004, respectively, showing a statistical difference (* $p < 0.05$). Interestingly, the difference between nondoped (0.015 ± 0.005) and GO-doped hydrogels (0.011 ± 0.003) was lower in the case of synthetic synovial fluid, without a significant statistical difference (Figure 4c). Moreover, the COF values of GG/PEGDA10_5 minUV_10 min$MgCl_2$ tested in the two conditions (PBS and synthetic synovial fluid) were statistically different (** $p < 0.01$). Overall, COF values are within the range of native articular cartilage tissue, and the presence of GO improved the lubrication properties of the superficial cartilage zone-mimicking hydrogel. However, such a difference was not statistically significant in the case of the synthetic synovial fluid, probably due to a high a priori lubrication due to the fluid, which did not allow to discriminate the differences between the two hydrogel formulations.

The COF was also analyzed by testing further normal forces (5 and 10 N). Figure 4c shows an increment of COF values using both lubricants while increasing the normal forces: in PBS

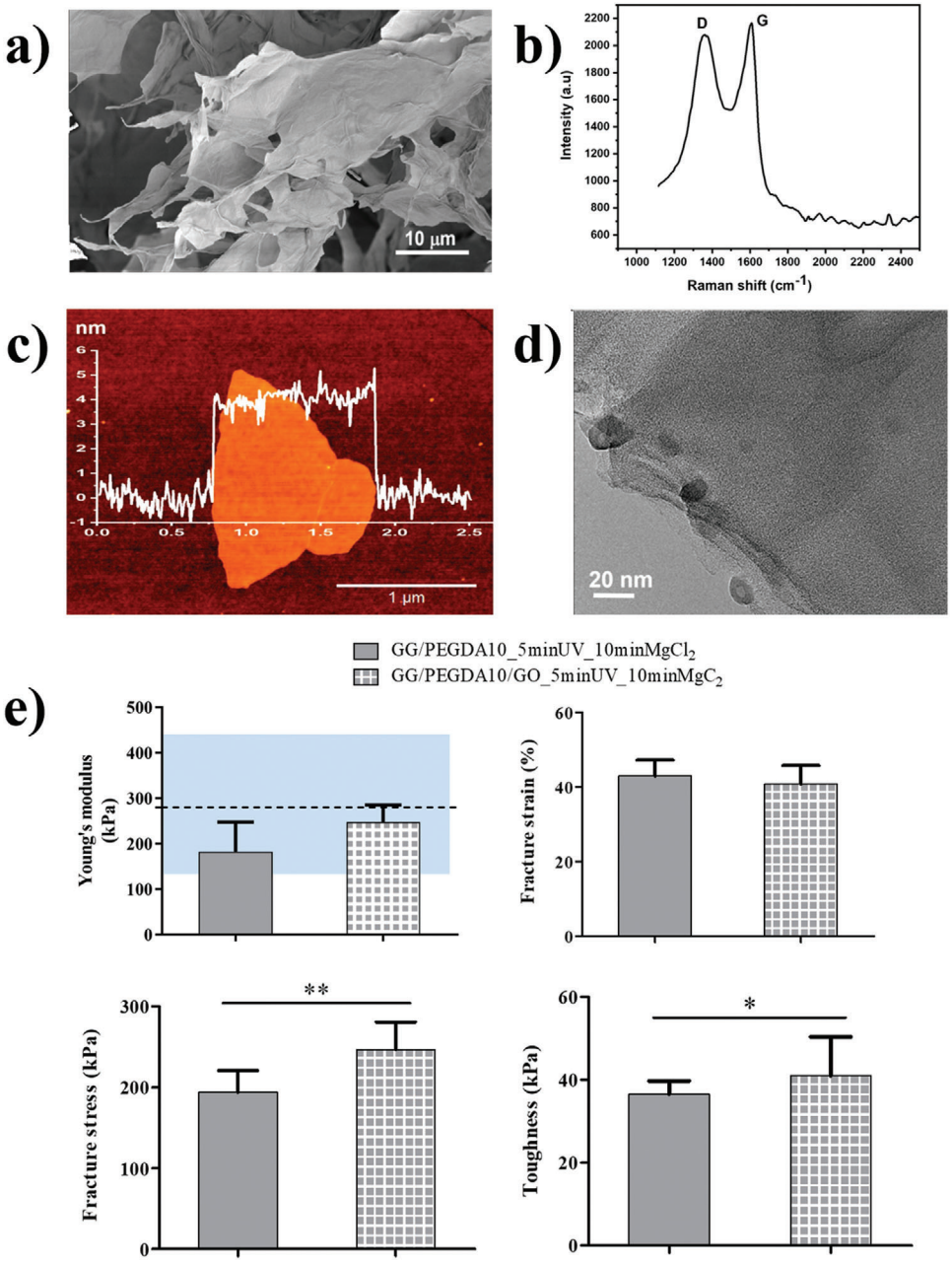

Figure 3. Characterization of GO and its inclusion in the hydrogel: a) SEM images of layered GO flakes; b) Raman spectrum at 532 nm; c) AFM measurements of a dispersed GO demonstrated minimal thickness of 4.0 ± 0.3 nm ($n = 5$); d) HRTEM image, confirming the layered structure of a dispersed GO. e) Analysis of the nanocomposite GG/PEGDA10/GO_5 minUV_10 minMgCl$_2$: Young's modulus, fracture stress, fracture strain, and toughness. For the Young's modulus, the blue areas represent the range of stiffness featuring the superficial articular cartilage, reported in ref. [5b]. Data presented as mean ± SD, $n = 5$, p-values are calculated using the Student's t-tests, * $p < 0.05$, ** $p < 0.01$. Analyzed samples: GG/PEGDA10_5 minUV_10 minMgCl$_2$, GG/PEGDA10/GO_5 minUV_10 minMgCl$_2$.

environment, the COF increased up to 0.031 ± 0.001 and 0.033 ± 0.001 respectively for the GO-doped and nondoped formulations, while in the case of synthetic synovial fluid the values increased up to 0.018 ± 0.004 and 0.025 ± 0.003 respectively for the GO-doped and nondoped formulations. Notably, statistically significant differences were also found between either lubricant in the case of 10 N for both GO- (** $p < 0.01$) and nondoped hydrogels (* $p < 0.05$). The largest difference between GO-doped and non-doped samples was observed in the case corresponding to the highest normal force applied (10 N).

Finally, Figure 4d reports the wear-related results obtained by applying a force of 0.5 N at a rotational speed of 0.05 min^{-1} above the transition zone between static and kinematic regimes. The average value of COF for the GG/PEGDA10_5 minUV_10 minMgCl$_2$ hydrogel increased with an approximately linear trend from 0.026 to 0.041 (PBS lubricant) and from 0.015 to 0.032

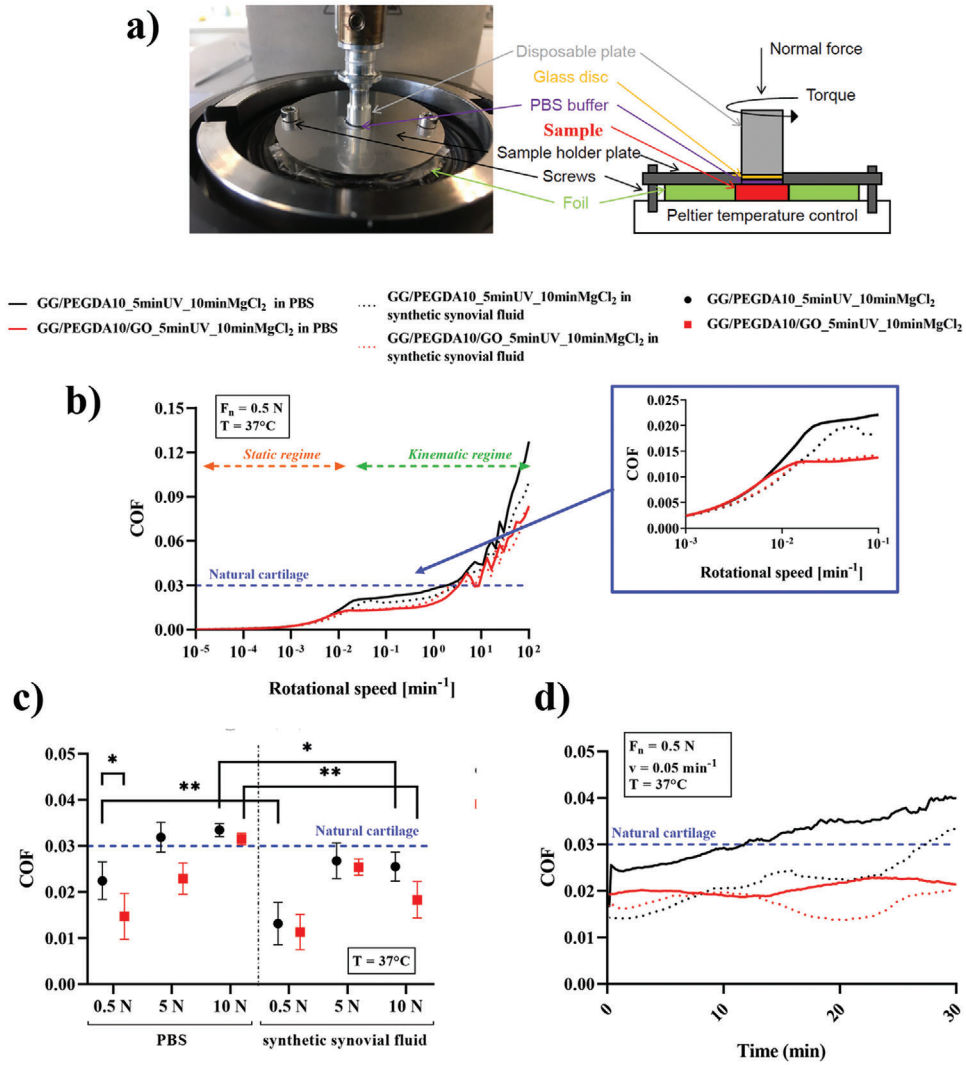

Figure 4. a) Depiction of the set-up used for testing the hydrogels (red block). b) Analysis of the composite hydrogels according to the Stribeck curve: static and dynamic regimes are marked with arrows, and the transition zone is magnified. Tests were performed evaluating both PBS and synthetic synovial fluid as lubricants. c) Values of coefficient of friction (COF) (mean ± SD) measured at the transition region varying the normal force (0.5, 5, and, 10 N). d) Analysis of the hydrogel wear upon the application of a constant normal force for 30 min at constant normal force (0.5 N) and rotational speed (0.05 mm^{-1}). All tests were performed at 37 °C. In all graphs, the blue line represents the COF of the healthy articular cartilage.[5b] Data presented as mean ± SD, $n = 3$, p-values are calculated using the Student's t-tests, * $p < 0.05$, ** $p < 0.01$. Analyzed samples: GG/PEGDA10_5 minUV_10 minMgCl$_2$, GG/PEGDA10/GO_5 minUV_10 minMgCl$_2$.

(synthetic synovial fluid). Differently, the GO-doped formulation showed an almost constant trend over time both in PBS (≈0.020) and synthetic synovial fluid (≈0.017). Interestingly, such values were always below the maximum COF of natural articular cartilage (0.03).

The role of GO as lubricant agent was furtherly confirmed in these experimental conditions, even if this aspect was more evident with PBS than synthetic synovial fluid. Probably, such a difference is ascribed to a "masking effect" due to the synthetic synovial fluid, which made the tribological test less sensitive toward the materials to be tested. This result contributed to demonstrate the lubricant properties provided by the addition of the GO within the polymeric network, even when subjected to a continuous mechanical solicitation. It is worth highlighting that the COF values found in the test were within the range featuring the natural articular cartilage,[5b] apart from the cases tested in PBS at 5 and 10 N. The evaluation of GO as a remarkable agent to reduce the coefficient of friction had been highlighted by Wang et al.[49] for zwitterionic poly(sulfobetaine methacrylated) (PSBMA) hydrogels, showing superior hydration lubrication capability.[50] In this study, the reduction of friction in PSBMA hydrogels with embedded GO nanosheets was confirmed by investigating two different lubricants (water and a lipid solution): in both cases, the doped formulations guaranteed lower COF than the bare ones. The ranges of COF found in this study are comparable with our results, even if the experimental conditions differed in terms of lubricant solutions employed, hydrogel chemistry and measurement set-up (ball-on-flat). It should be remarked that in this

paper a realistic situation is pursued, being the set-up properly customized to emulate the load applied to the cartilage in standard conditions.

The tribological properties of graphene mainly depend on its structure.[51] GO might exhibit a slightly larger COF than graphene caused by the presence of exposed interlayer hydrogen bonds, even if it confers a longer lifetime and wear life because it promotes layer slipping mechanisms. This is extremely important for bear-wearing applications, as in the field of materials for cartilage substitution. As demonstrated by Tang et al.,[52] GO with a relatively large lateral size guarantees lubrication by the sliding along the basal plane of its crystalline lamellar structure. The authors also identified a concentration threshold at 0.1% w/v, above which GO, similarly to other nanomaterials, starts decreasing its lubrication effect.[53]

The concentration of GO adopted in this work (0.01% w/v) is well below such a threshold value. Also, Meng et al.,[46b] investigated different concentrations of GO embedded into PVA nanocomposite hydrogels lubricated with FBS (up to 2% w/v). Their results showed that the minimum COF (close to 0.07) was found for the GO concentration of 1.5% w/v, while it resulted higher for all the other concentrations tested (above and below 1.5% w/v). It is important to underline that the lubrification properties achieved by these authors were inferior to the results reported in this work. Furthermore, the use of such a high concentration of GO (1.5% w/v) could severely influence cell viability due to cytotoxic effects.

Figure 4c shows the results of a wear test performed through a rheometer: it can be observed that for both samples, GG/PEGDA10_ 5 minUV_10 min$MgCl_2$ and GG/PEGDA10/GO_5 minUV_10 min$MgCl_2$, the thickness of the hydrogel remained relatively constant during the whole test, as well as the applied torque. The oscillation was probably due to the elastic deformation of the hydrogel specimen. Native AC possesses considerable lubricant properties in order to withstand the cyclical stresses due to the daily life activities of people. The addition of GO was demonstrated to be effective in keeping the COF at a value lower than the native AC one (0.03).[5b] Furthermore, the doped formulation did not show any preliminary signs of wear. Lubricity and wear represent crucial factors for many biomedical applications, especially those related to cartilage tissue substitution.[54]

2.3. Full Cartilage-Mimicking Bilayered Hydrogel

Figure 5a shows the fabrication procedure of bilayered hydrogels by sequentially adding each specific hydrogel formulation in a polydimethylsiloxane (PDMS) mold, while Figure S3 (Supporting Information) shows the transition between deep and superficial cartilage-mimicking hydrogels. The model described in the following permitted, by using the mechanical data reported in Section 2.1 to find appropriate volumetric proportions for building a bilayered hydrogel structure, whose overall properties could be similar to the ones of a healthy human AC (a full-thickness tissue, including all the different zones described in the Introduction section). It has been assumed that the composite material was isotropic and composed of two zones (deep and superficial), which contribute to the final stiffness of the composite material in direct proportion to their volume fraction.[55] The volumetric fraction of deep cartilage (f_{DC}) and superficial cartilage (f_{SC}) for cylindrical hydrogels is the ratio between the deep or superficial cartilage volume and the total volume, described as:

$$f_{DC} = \frac{V_{DC}}{V_{tot}} = \frac{\pi r^2 h_{DC}}{\pi r^2 h_{tot}} = \frac{h_{DC}}{h_{tot}} \quad (1)$$

$$f_{SC} = \frac{V_{SC}}{V_{tot}} = \frac{\pi r^2 h_{SC}}{\pi r^2 h_{tot}} = \frac{h_{SC}}{h_{tot}} \quad (2)$$

where r is the radius of the crosslinked hydrogel disc, h_{DC}, h_{SC} and, h_{tot} are the heights of deep cartilage, superficial cartilage, and the total disc (deep + superficial), respectively. Moreover, the relationship between deep and superficial volumetric fractions is:

$$f_{DC} + f_{SC} = 1 \quad (3)$$

The equivalent Young's modulus of the bilayered structure can be expressed by applying the Reuss model as follows:

$$E_{cartilage} = \frac{E_{DC}\, E_{SC}}{f_{SC}\, E_{DC} + f_{DC}\, E_{SC}} \quad (4)$$

where $E_{cartilage}$, E_{DC} and, E_{SC} are the Young's modulus of the healthy cartilage, the one of the deep cartilage hydrogel, and the one of the superficial hydrogel, respectively.

Substituting the relationship (3) in (4), f_{deep} can be obtained as:

$$f_{DC} = \frac{E_{DC}\, E_{SC}}{E_{cartilage} - E_{SC}} * \frac{1}{E_{SC} - E_{DC}} \quad (5)$$

Subsequentially, $f_{DC}$was substituted in (1) to find h_{DC} as:

$$h_{DC} = f_{DC}\, h_{tot} \quad (6)$$

Finally, the expression (6) was substituted into the definition of h_{tot} to calculate h_{SC} as:

$$h_{SC} = h_{tot} - h_{DC} \quad (7)$$

Fixed any height, to calculate the volumetric fractions of deep and superficial layers, E_{DC} and E_{SC} were considered equal to 864 and 182 kPa, respectively (data derived from the mechanical characterization of hydrogels), while $E_{cartilage}$ was considered equal to 500 kPa, based on literature data.[5b,56]

Using the model, we obtained the volumetric fraction of the superficial (GG/PEGDA10/GO_5 minUV_10 min$MgCl_2$) and deep (GG/PEGDA15_5 minUV_10 min$MgCl_2$) layers equal to 19.43% and 80.57%, respectively. This analysis partially reflects the real situation of native AC, in which the superficial layer constitutes the 10–20% of the overall cartilage thickness.[57]

In the state-of-the-art, similar models were developed for predicting composite hydrogel moduli, once given the mechanical properties of the different constitutive materials. Previous studies reported the use of a model to calculate the volumetric fraction of sol–gel composites.[58] Isostress within

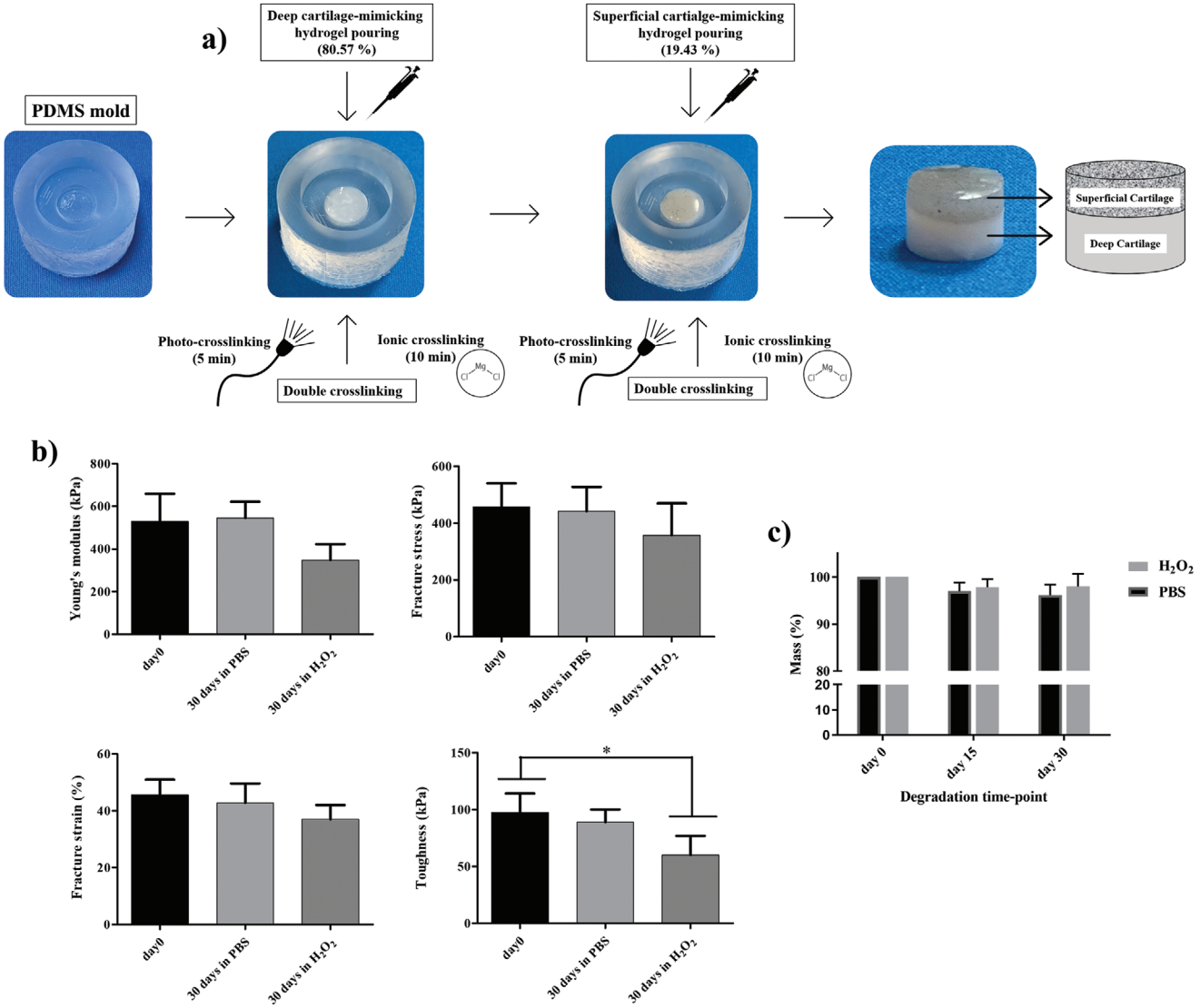

Figure 5. a) Depiction of the sequential fabrication procedure used to fabricate the cylindrical bilayered hydrogels by exploiting a PDMS mold. b) Mechanical analysis of the bilayered hydrogels after 30 d incubation in PBS and H_2O_2 in terms of: Young's modulus, fracture stress, fracture strain and toughness. c) Analysis of the total mass variation overtime, upon incubation in PBS and H_2O_2. Data are presented as mean ± SD, $n = 4$, p-values are calculated using the one-way ANOVA with Tukey's post-test correction, * $p < 0.05$. Analyzed sample: full cartilage-mimicking bilayered hydrogel composed of GG/PEGDA10_5 minUV_10 min$MgCl_2$ (bottom part) and GG/PEGDA10/GO_5 minUV_10 min$MgCl_2$ (top part).

isostrain models were used to describe the mechanical behaviors of poly(2-acrylamido-2-methylpropanesulfonic sodium) (PNaAMPS) dispersed into neutral polyacrylamide (PAAm) hydrogels at small deformation.[58c] Moreover, an isostress model was developed and validated to predict the mechanical responses of cellulose nanocrystals (CNC)-reinforced poly(2-hydroxyethyl methacrylate) (PHEMA) nanocomposite hydrogels.[58a] However, no multilayered structures using different materials or different concentrations of blended materials have been modeled to predict their whole elastic modulus, in the field of cartilage substitution.

Once fabricated, the mechanical characterization of the bilayer was performed to compare the consistency of the model results with the experimental ones, also evaluating the stability of the hydrogel after incubation in physiological medium (PBS) or inflammatory-like conditions (H_2O_2) up to 30 d. Interestingly, the average Young's modulus of the bilayer (529 ± 128 kPa) was very close to the value of the healthy AC (500 kPa), used to apply the model. As shown in Figure 5c, the Young's modulus, fracture stress, fracture strain, and toughness did not vary after one month in PBS. Slightly more evident differences were found after incubation in H_2O_2, especially regarding toughness. H_2O_2 accounts for a more aggressive condition, used to predict long-term oxidative degradation through a short-term test. Indeed, induced oxidative stresses can affect both GG and PEGDA.[59] However, even the most affected parameter, namely the toughness, remained close to the one owned by the native AC, namely about 47 kPa,[60] also in the worst case. These results demonstrate that

one month of incubation produced no marked mass loss in the tested samples, even if there was a slight effect on the material mechanical properties, induced by the oxidative stresses of H_2O_2. Probably, a change of the polymer chain interactions might occur during the continuous presence of an inflammatory condition.

2.4. Wear Test

To perform a wear test, the bilayered hydrogels described in the previous section were fabricated within a menisci-like phantom, as described in **Figure 6**a.

The wear test was performed using a four-station displacement control knee joint simulator under fetal bovine calf serum-based solution that mimics the knee synovial fluid. A vertical load was applied and the test run with a frequency of 1.1 Hz.[61] The applied load at a frequency of 1.1 Hz described a full walk step that was simultaneously composed of four different knee movements (trends), namely axial force, flexion-extension angle, intra-extra tibial rotation, and front-rear motion. Figure 6b reports a general description of the system components and some sequential pictures of the system while performing the test. A movie of the knee simulator during the wear test is reported as Movie S1 (Supporting Information).

Macroscopic visual examination of all knee-retrieved components revealed a consistent wear pattern between two subsequentially ISO 14243 standard wear tests, as shown in Figure 6c–e. A similar behavior was observed between the medial and the lateral condyles of the specimens. After 18 000 cycles, we observed that both condyles remained perfectly intact (Figure 5d) both in the center and at the edges, as the pretest samples (Figure 6c). After 100 000 cycles on the UHMWPE holes, we observed that the medial condyle showed some slight signs of wear without delamination, while the lateral condyle remained intact (Figure 6e). We can suppose that medial condyle hydrogel samples were subjected to delamination due to rubbing with the prosthesis because the body load is transmitted through the menisci in different proportions (70% in the lateral compartment and 50% in the medial compartment).[62] Moreover, this effect can be also partially due to a scarce adhesion between the UHMWPE hole and the hydrogel, being the PE hydrophobic. No statistical differences were found in terms of roughness between 100 000 cycles-tested and pretested samples (Figure 6f), while slight signs of wear were observed on the surface of the stressed hydrogel (Figure 6g). Despite the presence in the state-of-the-art of different examples of cartilage-substituting hydrogels, to our knowledge, our study is the first one assessing the functional behavior of the produced hydrogels by using this wear test, adhering to the ISO 14 243 standard. Thus, these results shed light on the cyclical resistance of the fabricated hydrogels, which is of crucial importance for assessing their possible success as an osteoarticular tissue substitute, but also highlight the need, in general, for an extensive assessment of the wear behavior of hydrogels, in the state-of-the-art of this research field.

The test was conducted by combining all different walk movements following the ISO 14243 standard for 100 000 cycles that corresponded to evaluate standard human continuous walk for around 24 h. To the best of our knowledge, this is the first study providing a set of such new hydrogels tested on a displacement control knee joint simulator designed to test knee prostheses. Vazquez et al.,[63] developed a novel in vitro model of damage through cartilage-on-cartilage cyclic loading without the use of a knee simulator. We chose to replicate a worst-case-scenario in order to assess the wear behavior of such new constructs. We can thus claim that the fabricated bilayer showed an excellent behavior when subjected to a high number of cycles and can thus be considered a suitable functional cartilage substitute. It must be highlighted, as a limitation of this study, that the wear test performed with the knee simulator has been not carried out with natural cartilage tissues: the authors relied on state-of-the-art data on natural cartilage, as a reference, although such tests were carried out in slightly different conditions. An extensive evaluation of the natural cartilage properties assessed with the simulator reported in this work and a comparison with the previously mentioned state-of-the-art data could be the focus of a future study.

It is important to underline that the materials described in this study could be injected directly in chondral defects through syringes-like devices and sequentially crosslinked in situ.[64] Indeed, we preliminarily evaluated the printability of both hydrogel formulations mimicking the deep and the superficial cartilage zones, finding encouraging results (Figure S4, Movie S2, Supporting Information). However, the potential application of such a bilayered hydrogel does not exclude the fabrication of the construct outside the body and its subsequent surgical implantation (e.g., through arthroscopic procedures). Along this line, the use of computed tomography (CT) data would help in obtaining the exact shape of chondral defects and then to fabricate defect-specific tissue substitutes using customized molds.[65]

2.5. Cytotoxicity Evaluation

Finally, to evaluate the cytotoxicity of the superficial and deep hydrogels (GG/PEGDA10/GO_5 minUV_10 min$MgCl_2$ and GG/PEGDA15_5 minUV_10 min$MgCl_2$), we assessed viability and metabolic activity of human chondrocytes put in contact with the supernatant collected from both hydrogels incubated in culture medium for 24 h. Cell viability and cell metabolic activity were checked after two and six days. Cell viability assessed by live and dead (L/D) assay showed the presence of only viable cells (green stained), almost without dead cells (red stained) at the analyzed time points in both experimental groups, indicating that the hydrogel formulations did not affect cell viability (**Figure 7**a). The behavior was similar among the cells put in contact with the hydrogel-derived media and the cells cultured as a control group (chondrocyte simply grown in standard culture medium).

Furthermore, metabolic cell activity, evaluated by MTT assay, showed no statistical difference at the two time points between the control and the experimental groups (Figure 7b). After 6 d, the absorbance values were all lower than the ones found after 2 d. This result was due to cell confluence after a week in culture, that determined a reduced metabolic activity in all samples analyzed, without any difference between control and experimental groups.[66]

Cytocompatibility is a fundamental standard evaluation of cell viability for cartilage repair. Our data confirmed that the

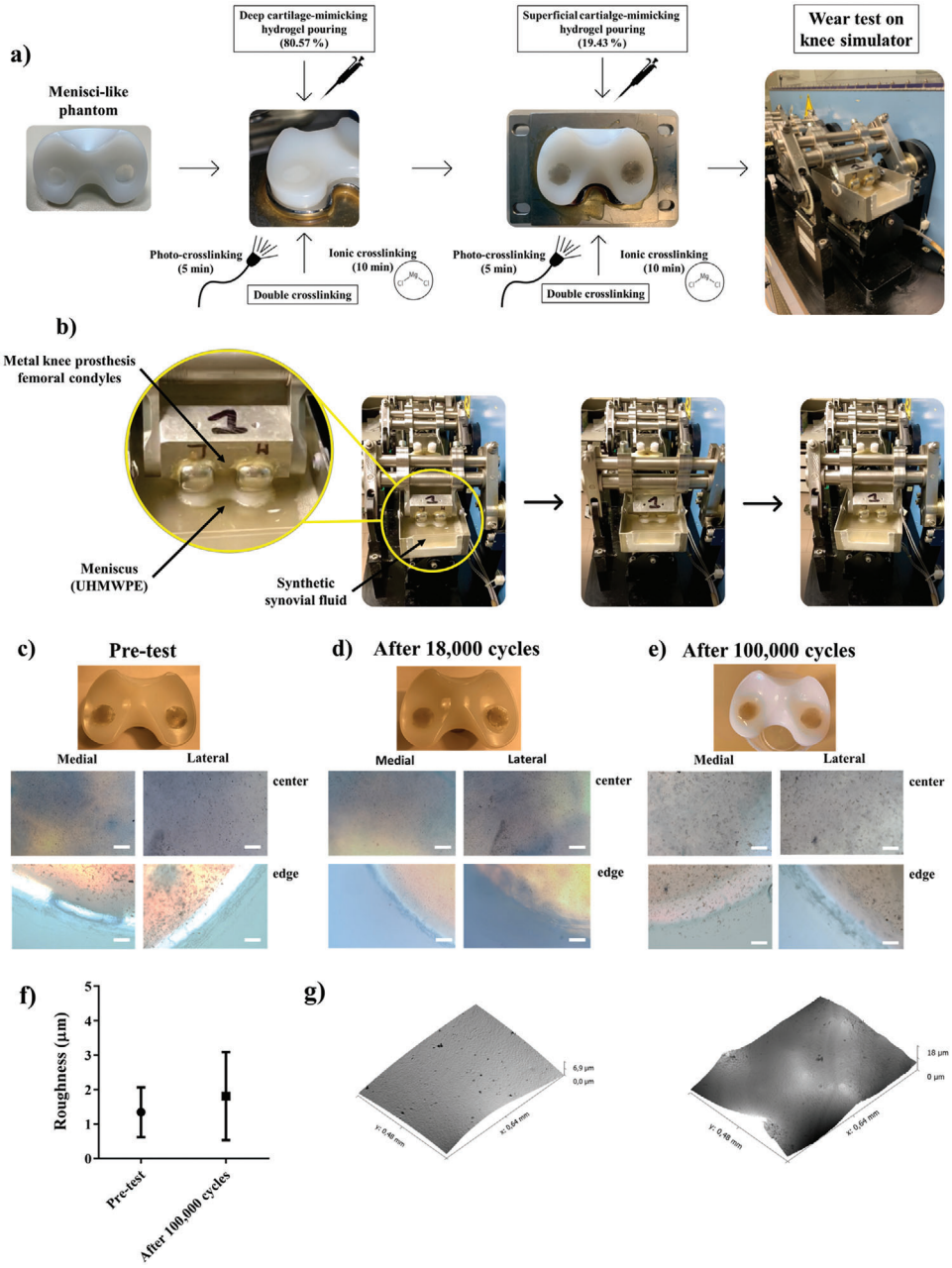

Figure 6. a) Depiction of hydrogels fabrication within a menisci-like phantom. b) Depiction of the knee simulator set-up. Sequential images of the knee simulator movements during the wear test (see also Movie S1, Supporting Information). In the zoomed image, it is possible to observe that the meniscus is immersed into fetal bovine calf serum-based solution and loaded by femoral condyles of metal knee prosthesis. c) Macroscopic and brightfield (4×) images of samples before wear test. d) Macroscopic and brightfield (4×) images of samples after 18 000 cycles. e) Macroscopic and brightfield (4×) images of samples after 100 000 cycles. The brightfield images of medial and lateral condyles were captured in the center and on the edge of samples using an optical microscope. Scale bar: 250 µm. f) Average roughness measurements using optical profilometer of pretested and tested (100 000 cycles) bilayered hydrogels. g) Surface images captured using optical profilometer of pre-tested (left) and tested (right) bilayered hydrogels. Data presented as mean ± SD, $n = 4$, p-values are calculated using the Student's t-tests. Analyzed sample: full cartilage-mimicking bilayered hydrogel composed of GG/PEGDA10_5 minUV_10 min$MgCl_2$ (bottom part) and overlapped GG/PEGDA10/GO_5 minUV_10 min$MgCl_2$ (top part).

hydrogels did not affect this important parameter. Only three papers focused on different combinations of GG/PEGDA[35,67] and GG/GO,[68] but cell viability was evaluated only in GG/PEGDA hydrogels. In line with our data, they have demonstrated that mesenchymal stromal cells embedded in GG/PEGDA showed a high percentage (above 87%) of viable cells.[35] By contrast, other authors have shown that a different GG/PEGDA hydrogel formulation provided an unfavorable environment for mesenchymal stromal cells proliferation associated to an increase of cell apoptosis starting from third day.[67]

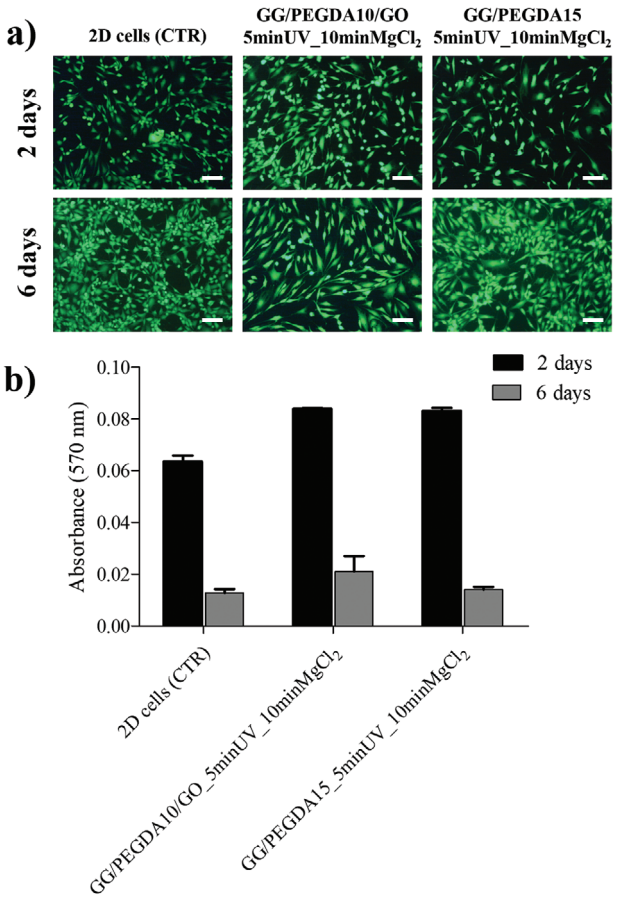

Figure 7. a) Live/dead images of 2D chondrocytes untreated (CTR), treated with GG/PEGDA10/GO_5 minUV_10 min$MgCl_2$ supernatant, and treated with GG/PEGDA15_5 minUV_10 min$MgCl_2$ supernatant evaluated after 2 and 6 d. Viable cells are shown in green dead/necrotic cells are shown in red. Scale bars: 200 µm. b) MTT test of the same samples evaluated after 2 and 6 d. Data presented as mean ± SD, $n = 4$, p-values are calculated using the Student's t-tests. Analyzed samples: GG/PEGDA10/GO_5 minUV_10 min$MgCl_2$, GG/PEGDA15_5 minUV_10 min$MgCl_2$.

3. Conclusion

We described the development of a bilayered hydrogel able to mimic the mechanical and lubrication features of native AC. The bilayer was based on a combination of GG and PEGDA, and on two combined crosslinking approaches (physical and ionic). The resulting material proved to effectively modulate the mechanical properties of the superficial and the deep components of the bilayer. In this process, the influence of the ionic crosslinking was more relevant than the photo-crosslinking one. Two formulations were identified as the optimal ones to mimic the superficial and deep zones of the human articular cartilage.

GO nanosheets were synthesized in order to improve the lubrication properties of the top layer, thus to mimic the articular cartilage also in terms of low friction. Tribological analyses confirmed the beneficial effect of the addition of GO nanosheets into the top layer. Future efforts may be focused on evaluating the tribological properties of the hydrogel–hydrogel interface, as well as possible interactions of the hydrogel with different materials that could be used for prosthetics purposes (steel, PTFE, etc.). The nanocomposite also guaranteed improved mechanical properties, especially toughness.

By applying the Reuss model, we developed a bilayer structure mimicking the overall mechanical properties of the healthy articular cartilage, using two layers made of different hydrogel formulations and featured by specific thicknesses, which resulted as the output of the model. No cytotoxic effects were found on human chondrocytes up to 6 d, demonstrating the safety of the bilayered hydrogel. Moreover, a wear test confirmed that the bilayered construct can withstand physiologically relevant stresses up to 100 000 cycles. In conclusion, the proposed biomimetic bilayered hydrogel is a promising candidate as a possible synthetic substitute to be delivered into chondral and osteo-chondral defects in a minimally invasive way and to restore the functional properties of the cartilage. Future in vivo tests will demonstrate the pre-clinical and clinical suitability of such a composite material.

4. Experimental Section

Materials: Gellan gum (GG) powder (Gelzan, Merck) and poly (ethylene glycol) diacrylate (PEGDA, Mn: 575, Merck) solution was used for the preparation of hydrogels. 2-hydroxy-4′-(2-hydroxyethoxy)-2-methylpropiophenone (Irgacure 2959, I2959, Merck) was used as photoinitiator, stocked in a mother solution made of dimethyl sulfoxide (DMSO, Merck). Magnesium chloride hexahydrate ($MgCl_2$-$6H_2O$, Merck) diluted in deionized water was used to perform the ionic crosslinking of hydrogels. Graphite flakes (99%, Alfa Aesar), H_2SO_4 (98%, Merck), H_3PO_4 (98%, Merck), $KMnO_4$ (99%, Merck) and H_2O_2 (30% Merck) were used to synthesize graphene oxide (GO) sheets. Wear tests were conducted using sodium azide (NaN_3, Merck) and ethylenediaminetetraacetic acid (EDTA, Merk). Cell culture studies were conducted using low glucose Dulbecco's modified Eagle medium (DMEM, Merk), fetal bovine serum (EuroClone), penicillin/streptomycin (Gibco) and trypsin/EDTA (EuroClone, Merk). Cell viability studies performed using phosphate buffered saline (PBS, Gibco) solution, live/dead viability/cytotoxicity kit (Invitrogen) and metabolic activity by 3-(4,5-dimethyl-2-thiazolyl)-2,5-diphenyl-2H-tetrazolium bromide (MTT, Merck).

Preparation of Superficial and Deep Cartilage Hydrogels: Briefly, GG (1.75 and 1.67% w/v) was dissolved in deionized water by magnetic stirring at 65 °C for 1 h. After dissolution, the solutions were formed by adding PEGDA at a concentration of 15% and 10% w/v, respectively. Both solutions were kept at 75 °C and agitated by magnetic stirring for 1 h. Then, I2959 photoinitiator (0.1% w/v) was added in both solutions by maintaining both temperature control and magnetic stirring active. Finally, each formulation was poured into cylindrical holes (diameter: 6 mm; height: 5 mm) of a custom-made PDMS mold. The photo-crosslinking was performed by UV light exposure using a UV optic fiber ($\lambda = 365$ nm, Lightning cure LC5, Hamamatsu Photonics UK, Ltd) at an intensity of 40 mW cm^{-2} for 5 and 10 min. Some hydrogels underwent a further ionic crosslinking step through a first immersion into a $MgCl_2$ solution (1% w/v in deionized water) for 10 minutes at room temperature (RO). Then, all the sample was finalized by incubation in DMEM for 24 h at 37 °C. All combinations of materials at different concentrations and crosslinking approaches are summarized in Table S1 (Supporting Information).

Hydrogels Mechanical Characterization: Each sample type was analyzed in terms of Young's modulus (E), fracture stress, fracture strain, and toughness. Uniaxial compression was performed with a Instron Mechanical Testing System (model 2444, Instron, Norwood, MA, USA) equipped with both ± 10 N and ± 1000 N load cells at a compression rate of 1 mm min^{-1} until reaching the hydrogel breaking point. E derived from the linear

region of the stress-strain curve (the first 10% of strain), fitted according to the equations:

$$\sigma = \frac{F}{A_0} \tag{8}$$

and

$$\varepsilon = \frac{\Delta l}{l_0} \tag{9}$$

where σ and ε are the stress and the strain, F is the force, Δl is the deformation, A_0 is the sample area and l_0 is the sample initial length. E was calculated according to the equation:

$$E = \frac{\sigma}{\varepsilon} \tag{10}$$

The fracture stress and fracture strain were assumed as the stress and strain at which the sample broke. The toughness, defined as the amount of strain energy per unit volume that a hydrogel can absorb, was calculated as the area under the stress-strain curve up to the breaking point.

The swelling ratio was assessed to measure the amount of water absorbed by each type of hydrogel. The mass of each sample type was measured after incubation in DMEM for 24 h at room temperature after removing residual liquid using filter paper ($W_{\text{after swelling}}$). Then, each sample was dried entirely, and the mass was weighed (W_{dry}). The calculation of swelling ratio follows the equation:

$$\text{SR} = \frac{W_{\text{after swelling}}}{W_{\text{dry}}} \tag{11}$$

Graphene Oxide Synthesis and Characterization: GO was synthesized, as described in the previous paper.[69] In short, graphite flakes were oxidized using the modified Hummer's method.[42] A 9:1 mixture of concentrated H_2SO_4/H_3PO_4 (360:40 mL) was added to a mixture of graphite flakes (3 g) and $KMnO_4$ (18 g). The reaction was then heated to 50 °C and stirred for 12 h. Next, the reaction was cooled to room temperature and decanted onto ice (400 mL) with 30% H_2O_2 (3 mL). For workup, the mixture was washed by extensive centrifugation cycles with water (12 000 rpm for 4 h) following by a dialysis for a week. When the solution pH was reached to pH = 7, it was centrifuged again (12 000 rpm for 4 h), and finally dried by lyophilization, yielding 5 g of graphite oxide. The obtained graphite oxide (yellowish solid) was exfoliated to GO sheets by half an hour of ultrasonication (brown solution).

The GO bulk was characterized by field-emission SEM (FESEM; FEI, Helios 600) operating at 5 keV. HRTEM measurements were carried out by a JEOL-2100 instrument operating at 200 keV. HRTEM samples were prepared by dispersing a section of GO bulk in ethanol followed by a gentle sonication for 15 min; then a single droplet of the dispersion on a 300-mesh Cu lacey carbon grid (from SPI) was drop casted. Raman scattering data in the range of 1000–3000 cm^{-1} was taken using a micro-Raman instrument (HORIBA Scientific LabRAM HR) in the air at RT. GO bulk sample was excited by a laser with an excitation wavelength of $\lambda_{ex} = 532$ nm. AFM measurements were performed by using a Bio FastScan scanning probe microscope (Bruker AXS). All images were obtained using soft tapping mode with a Fast Scan B (Bruker) silicon probe (spring constant of 1.8 N m^{-1}). The resonance frequency of the cantilever was approximately 450 kHz (in the air). The measurements were performed under environmental conditions. The images were captured in the retrace direction with a scan rate of 1.6 Hz. The resolution of the images was 512 samples per line. For image processing, Nanoscope Analysis software was used. The "flatting" and "planefit" functions were applied to each image. GO flakes were measured on Si/SiO_2 wafer, prepared by a single droplet from the same dispersion of GO as before.

Preparation of Nanocomposite Hydrogels: GO sheets were resuspended in deionized water (0.2% w/v) and deagglomerated using an ultrasonic bath (Bransonic 2510, power: 20 W) for 5 min before their use. Then, the GO suspension was added to the GG/PEGDA10_5 minUV_10 min$MgCl_2$ hydrogel solution to get a final concentration of 0.01% w/v and the blend (GG/PEGDA10/GO_5 minUV_10 min$MgCl_2$) was stirred at 75 °C for 30 min for obtaining a homogenized solution. After that, the solution was poured into cylindrical holes (diameter: 6 mm; height: 5 mm) of a custom-made PDMS mold and photo-crosslinked upon UV exposure (same parameters described in Section 5.2). Later, the ionic crosslinking was performed on some hydrogels by immersing the samples in $MgCl_2$ solution (1% w/v in deionized water) for 10 min. Then, the ionic crosslinking was finalized by incubation in DMEM for 24 h at 37 °C.

A preliminary evaluation of GO nanosheets dispersion in the nanocomposite hydrogel was carried out using an optical microscope (Hirox digital microscope, Hirox Co Ltd.).

Characterization of GO-Based Nanocomposite Hydrogels—Mechanical Characterization

Young's modulus, fracture stress, fracture strain, and toughness and swelling ratio were measured as described in section "Hydrogels mechanical characterization".

Characterization of GO-Based Nanocomposite Hydrogels—Tribological Test: Tribological tests on crosslinked hydrogels with (GG/PEGDA10/GO_5 minUV_10 min$MgCl_2$) and without GO (GG/PEGDA10_5 minUV_10 min$MgCl_2$) (Figure 4a) were performed using a MCR 102 rheometer (Anton Paar) equipped with the Tribocell T-PTD200 and a Peltier temperature control, the H-PTD200 hood and a disposable measuring system shaft. Customized sample holders were used to keep fixed the specimens on the top of the Tribocell. The test geometry was set as flat-on-flat, in which a glass disc mounted on the shaft was interfaced to the surface of the hydrogel while lubricating the contact between these components with lubricants. The glass disc was pressed against the sample by applying a normal force. The COF was determined as the ratio between the frictional force and the normal force. A representation of the tribological set-up is shown in Figure 4a. During all experiments, the temperature was kept at 37 °C. Tests were performed by evaluating two types of lubricants: PBS (1×) and a synthetic synovial fluid, according to the ISO 14243. It was composed of 25% sterile FBS balanced with deionized water, 0.2% NaN_3 and 20×10^{-3} M EDTA.

The tribological tests were divided into three parts:

1) The normal force was applied and remained constant ($F_n = 0.5$ N)[70] during the entire test. The time for adjusting the normal force was kept short (1.5 min) to avoid potential evaporation of lubricants.
2) The first and second extended Stribeck curve runs were performed for running-in. The rotational speed was increased logarithmically from 10^{-5} to 10^{2} min^{-1}. Then, the third run was used for the final evaluation. Three tests consisted of three consecutive runs each, and the up-curve was considered for the analysis. The COF was evaluated by varying the force (0.5, 5, and 10 N) that corresponded to a different contact pressure (6.4, 63.7, and 127.4 kPa) on the hydrogel.
3) The wear behavior was investigated at a constant rotation speed (ν = 5 min^{-1}) for 30 min.

Development of Bilayered Hydrogels—Preparation of the Bilayered Structure

Bilayered structures were fabricated using the custom-made PDMS mold (diameter: 6 mm; height: 5 mm), assuming the volumetric ratios defined into the modeling. First, 113 µL of GG/PEGDA15_5 minUV_10 min$MgCl_2$ hydrogel solution was poured in the mold to achieve a height of 4 mm. Then, the hydrogel solution was photo-crosslinked upon UV light exposure for 5 min and after immersed in $MgCl_2$ solution (1% w/v, in deionized water) for 10 min. Subsequently, 28 µL of the nanocomposite GG/PEGDA10/GO_5 minUV_10 min$MgCl_2$ was poured onto the crosslinked DC layer to achieve a final height of 5 mm. Then, the bilayer

was photo-crosslinked upon UV light exposure for 5 min and after immersed in $MgCl_2$ solution (1% w/v, in deionized water) for 10 min. Finally, the crosslinked bilayered structures were incubated for 24 h at RO in DMEM.

Development of Bilayered Hydrogels—Characterization of Bilayered Structures: Young's modulus, fracture stress and strain and toughness were measured after preparation, as previously described in Section 5.3. The degradation of the bilayered structures was evaluated by incubating each sample at 37 °C in PBS (1×) and H_2O_2 (3% in PBS), according to the ISO10993-13, within an orbital agitator (711CT, Elettrofor).[71] A cyclic agitation at 2 rpm was imposed for the whole testing period. The material degradation kinetics was evaluated by monitoring the percentage of dry weight loss over time, after 2 weeks and 1 month. Four independent samples for each material type were tested.

The mechanical performance of the bilayered structures was also analyzed after 1 month of degradation in PBS and H_2O_2 and compared to those owned by the material without being subjected to degradation.

Development of Bilayered Hydrogels—Wear Test: Wear test was carried out to qualitatively evaluate whether the construct remained intact under repeated cyclical stresses. In particular, the wear test was performed using a four-station displacement control knee joint simulator (Shore Western, Inc., Monrovia, CA, USA) that consents to simulate the knee movement up to four degree-of-freedom (DOF), as previously reported.[61] Briefly, the menisci were sterilized with ethylene oxide (ETO) gas and tested in conjunction with four CoCrMo alloy femoral and tibial components (size 2; Adler ORTHO, Milan, Italy), consolidated by compression molding (accordingly to ISO 5834/1-2) and ETO sterilized. Four bilayered structures were prepared keeping the same volumetric ratio as described previously into two symmetric holes (diameter: 12 mm; height: 7 mm) created into ultrahigh-molecular-weight-poly-ethylene (UHMWPE) mobile menisci (Genus mobile bearing, size 2, Adler ORTHO, Milan, Italy). Axial load was applied vertically (perpendicular to the tibial tray), oscillating between 168 and 2600 N following the calculated profile. The applied kinematics was derived from the displacement control simulator. In particular, the flexion/extension angle oscillating between 0° (neutral) and 60° (flexion) was synchronously with the load; the anterior/posterior translation oscillating between −6.0 mm (neutral) and 6.0 mm (posterior), and the intra/extrarotation oscillating between −2.0 (extra-rotation) and 6.0° (intrarotation). The test was performed using fetal bovine calf serum as a medium and using a frequency of 1.0 ± 0.1 Hz, following the ISO 14243. Each test was performed in the presence of 25% sterile FBS balanced with deionized water and 0.2% NaN_3 to slow down bacterial growth, and 20×10^{-3} M EDTA to minimize precipitation of calcium phosphate. The wear test lasted 100.000 cycles. Macroscopic and brightfield (4×) images of all pretested and tested sample was captured using a professional camera and optical microscope (Nikon 90i, Nikon, Japan). The brightfield images of medial and lateral condyles were captured in the center and on the edge of samples using an optical microscope.

An optical profiler (Leica DCM8) was used to analyze the roughness of the bilayered hydrogels in the hydrated state before and after the wear test. Z-stacks (scan area 640 × 480 μm^2) were acquired, then data were converted into 2D images provided with a height-related greyscale and the surface roughness was estimated. The analysis was carried out by using the Gwyddion software (http://gwyddion.net/). The average roughness (R_a) was measured on the acquired images. Three Z-stacks were acquired for each sample type in its medial and lateral condyles.

Development of Bilayered Hydrogels—Cytotoxicity Evaluations: To perform in vitro cytotoxicity tests, the selected crosslinked GG/PEGDA15_5 minUV_10 min$MgCl_2$ and GG/PEGDA10/GO_5 minUV_10 min$MgCl_2$ hydrogels were incubated for 24 h in cell culture medium composed of DMEM with 10% FBS and 100 U mL^{-1} penicillin/streptomycin (3 mL per sample). The supernatants were collected and used for the analysis of the cell behavior for the following assays.

The human cell donors gave their informed, written consent prior to this study, and the study was approved by Istituto Ortopedico Rizzoli's ethics board (project number 814413). Isolated human OA chondrocytes (from male, 59 years old) collected into the biobank of Laboratory of Immunorhematology and Tissue Regeneration (at Istituto Ortopedico Rizzoli) were thawed and expanded in culture. Chondrocytes at passage three were seeded in eight wells chamber slides at a cell density of 1.2×10^4 cells per well. Cells were left to adhere for 24 h, then the culture medium was removed, and the supernatants collected from the GG/PEGDA15_5 minUV_10 min$MgCl_2$ and GG/PEGDA10/GO_5 minUV_10 min$MgCl_2$ hydrogels (500 µL per well) were transferred on the chamber slides. An untreated control was performed by simply changing the cell culture medium (DMEM, 10% FBS, 100 U mL^{-1} penicillin/streptomycin).

Cell morphology and viability were evaluated after 2 and 6 d by live/dead cell viability assay.[72] Cells were washed twice with PBS and then incubated with Ethidium homodimer-1 (4×10^{-6} M) and Calcein AM (2×10^{-6} M) for 45 min at 37 °C and 5% CO_2. Labeled cells were then visualized under an optical microscope (Nikon, Japan) for evaluating general morphology, viable (green) and dead (red) cells.

The MTT metabolic activity assay determined the ability of viable cells to reduce the yellow tetrazolium salt (MTT) to blue-colored formazan crystals by mitochondrial enzymes, detectable with a spectrophotometer. MTT metabolic activity assay was performed at the same time points (2 and 6 d). Cells were washed twice with PBS and then incubated with MTT for 3 h at 37 °C and 5% CO_2. Afterward, MTT solution was removed and HCl (0.1 M) was added to cells to permit redox reaction in formazan. Absorbance at 570 nm was evaluated using a spectrophotometer (Tecan, Life Science).

Statistical Analysis: Normality tests (D'Agostino-Pearson) were performed on all experimental data to assess the type of data distribution. Results with normal distribution were expressed as mean ± SD. Data analysis was performed by applying the Student's t-tests to evaluate statistically significant differences between two sample types under analysis, while one-way ANOVA with Tukey's post-test was adopted for multiple comparisons. Statistical analysis was carried out using GraphPad Prism (v 8.0.2). The significance threshold was set at 5% (* $p < 0.05$) and 1% (** $p < 0.01$).

Supporting Information

Supporting Information is available from the Wiley Online Library or from the author.

Acknowledgements

D.T. and L.V. contributed equally to this work. This work received funding from the European Union's Horizon 2020 research and innovation program, grant agreement No 814413, project ADMAIORA (Advanced nanocomposite materials for in situ treatment and ultRAsound-mediated management of osteoarthritis).

Conflict of Interest

The authors declare no conflict of interest.

Data Availability Statement

Research data are not shared.

Keywords

cartilage lubrication properties, cartilage mechanical properties, cartilage substitutes, gellan gum, graphene oxide, hydrogels, polyethylene glycol diacrylate

Received: August 14, 2020
Revised: December 28, 2020
Published online: February 15, 2021

[1] L. M. Anthony, *Junqueira's Basic Histology*, LANGE Series, McGraw-Hill Medical, New York **2013**.
[2] a) A. J. Sophia Fox, A. Bedi, S. A. Rodeo, *Sports Health* **2009**, *1*, 461; b) C. B. Carballo, Y. Nakagawa, I. Sekiya, S. A. Rodeo, *Clin. Sports Med.* **2017**, *36*, 413.
[3] a) J. Antons, M. G. M. Marascio, J. Nohava, R. Martin, L. A. Applegate, P. E. Bourban, D. P. Pioletti, *J. Mater. Sci.: Mater. Med.* **2018**, *29*, 57; b) B. He, J. P. Wu, T. B. Kirk, J. A. Carrino, C. Xiang, J. Xu, *Arthritis Res. Ther.* **2014**, *16*, 205.
[4] J. S. Jurvelin, M. D. Buschmann, E. B. Hunziker, *Proc. Inst. Mech. Eng., Part H* **2003**, *217*, 215.
[5] a) R. Krishnan, S. Park, F. Eckstein, G. A. Ateshian, *J. Biomech. Eng.* **2003**, *125*, 569; b) G. O'Connell, J. Garcia, J. Amir, *ACS Biomater. Sci. Eng.* **2017**, *3*, 2657.
[6] S. Camarero-Espinosa, B. Rothen-Rutishauser, E. J. Foster, C. Weder, *Biomater. Sci.* **2016**, *4*, 734.
[7] K.-X. A. L. Hooi Yee Ng, Y. -F. Shen, *JSM Bone Jt. Dis.* **2017**, *1*, 1010.
[8] a) D. J. Hunter, S. Bierma-Zeinstra, *Lancet* **2019**, *393*, 1745; b) L. A. McMahon, F. J. O'Brien, P. J. Prendergast, *Regener. Med.* **2008**, *3*, 743; c) L. Zhang, J. Hu, K. A. Athanasiou, *Crit. Rev. Biomed. Eng.* **2009**, *37*, i1.
[9] M. A. Jeffries, *Osteoarthritis Cartilage* **2019**, *27*, 371.
[10] A. D. Pearle, R. F. Warren, S. A. Rodeo, *Clin. Sports Med.* **2005**, *24*, 1.
[11] a) J. A. Buckwalter, *Clin. Orthop. Relat. Res.* **2002**, *402*, 21; b) A. E. Peters, R. Akhtar, E. J. Comerford, K. T. Bates, *Sci. Rep.* **2018**, *8*, 5931.
[12] S. G. Walter, R. Ossendorff, F. A. Schildberg, *Arch. Orthop. Trauma Surg.* **2019**, *139*, 305.
[13] a) E. T. Hurley, C. D. Murawski, J. Paul, A. Marangon, M. P. Prado, X. Xu, L. Hangody, J. G. Kennedy, *Foot Ankle Int.* **2018**, *39*, 28s; b) A. Ng, K. Bernhard, *Clin. Podiatr. Med. Surg.* **2017**, *34*, 461; c) S. L. Sherman, E. Thyssen, C. W. Nuelle, *Clin. Sports Med.* **2017**, *36*, 489.
[14] S. Elder, H. Chenault, P. Gloth, K. Webb, R. Recinos, E. Wright, D. Moran, J. Butler, A. Borazjani, A. Cooley, *J. Biomed. Mater. Res. A* **2018**, *106*, 2251.
[15] a) K. P. Krafts, *Organogenesis* **2010**, *6*, 225; b) M. A. Heinrich, W. Liu, A. Jimenez, J. Yang, A. Akpek, X. Liu, Q. Pi, X. Mu, N. Hu, R. M. Schiffelers, J. Prakash, J. Xie, Y. S. Zhang, *Small* **2019**, *15*, 1805510; c) M. Zeng, S. Jin, K. Ye, *SLAS Technol.* **2018**, *23*, 301. https://doi.org/10.1177/2472630318760515247263031876051 5.
[16] H. Kwon, W. E. Brown, C. A. Lee, D. Wang, N. Paschos, J. C. Hu, K. A. Athanasiou, *Nat. Rev. Rheumatol.* **2019**, *15*, 550.
[17] L. Cipollaro, M. C. Ciardulli, G. D. Porta, G. M. Peretti, N. Maffulli, *Br. Med. Bull.* **2019**, *132*, 53.
[18] a) X. Zhou, T. Esworthy, S. J. Lee, S. Miao, H. Cui, M. Plesiniak, H. Fenniri, T. Webster, R. D. Rao, L. G. Zhang, *Nanomedicine* **2019**, *19*, 58; b) J. Idaszek, M. Costantini, T. A. Karlsen, J. Jaroszewicz, C. Colosi, S. Testa, E. Fornetti, S. Bernardini, M. Seta, K. Kasarełło, R. Wrzesień, S. Cannata, A. Barbetta, C. Gargioli, J. E. Brinchman, W. Święszkowski, *Biofabrication* **2019**, *11*, 044101; c) L. Costa, J. Silva-Correia, J. M. Oliveira, R. L. Reis, in *Osteochondral Tissue Engineering: Nanotechnology, Scaffolding-Related Developments and Translation* (Eds: J. M. Oliveira, S. Pina, R. L. Reis, J. San Roman), Springer International Publishing, Cham, Switzerland **2018**, p. 281; d) S. Zhang, L. Chen, Y. Jiang, Y. Cai, G. Xu, T. Tong, W. Zhang, L. Wang, J. Ji, P. Shi, H. W. Ouyang, *Acta Biomater.* **2013**, *9*, 7236; e) E. J. Sheehy, T. Vinardell, C. T. Buckley, D. J. Kelly, *Acta Biomater.* **2013**, *9*, 5484; f) K. Kim, J. Lam, S. Lu, P. P. Spicer, A. Lueckgen, Y. Tabata, M. E. Wong, J. A. Jansen, A. G. Mikos, F. K. Kasper, *J. Controlled Release* **2013**, *168*, 166; g) S. Jin-Hyung, L. Jung-Seob, K. J. Young, C. Dong-Woo, *J. Micromech. Microeng.* **2012**, *22*, 085014; h) Z. Jia, F. Zhu, X. Li, Q. Liang, Z. Zhuo, J. Huang, L. Duan, J. Xiong, D. Wang, *Mater. Sci. Eng., C* **2019**, *99*, 541.
[19] C. Gegg, F. Yang, *Acta Biomater.* **2020**, *101*, 196.
[20] L. Jiang, Y. Wang, Z. Liu, C. Ma, H. Yan, N. Xu, F. Gang, X. M. Wang, L. Zhao, X. Sun, *Tissue Eng., Part B* **2019**, 398. https://doi.org/10.1089/ten.TEB.2019.0100.
[21] S. D. Eswaramoorthy, S. Ramakrishna, S. N. Rath, *J Tissue Eng. Regener. Med.* **2019**, *13*, 908.
[22] H. Chen, A. d. B. F. B. Malheiro, C. van Blitterswijk, C. Mota, P. A. Wieringa, L. Moroni, *ACS Appl. Mater. Interfaces* **2017**, *9*, 38187.
[23] a) J. A. M. Steele, S. D. McCullen, A. Callanan, H. Autefage, M. A. Accardi, D. Dini, M. M. Stevens, *Acta Biomater.* **2014**, *10*, 2065; b) M. Castilho, V. Mouser, M. Chen, J. Malda, K. Ito, *Acta Biomater.* **2019**, *95*, 297.
[24] X. Ren, F. Wang, C. Chen, X. Gong, L. Yin, L. Yang, *BMC Musculoskeletal Disord.* **2016**, *17*, 301.
[25] J. T. Oliveira, L. Martins, R. Picciochi, P. B. Malafaya, R. A. Sousa, N. M. Neves, J. F. Mano, R. L. Reis, *J. Biomed. Mater. Res., Part A* **2010**, *93A*, 852.
[26] a) D. F. Coutinho, S. V. Sant, H. Shin, J. T. Oliveira, M. E. Gomes, N. M. Neves, A. Khademhosseini, R. L. Reis, *Biomaterials* **2010**, *31*, 7494; b) J. Silva-Correia, J. M. Oliveira, S. G. Caridade, J. T. Oliveira, R. A. Sousa, J. F. Mano, R. L. Reis, *J. Tissue Eng. Regener. Med.* **2011**, *5*, e97.
[27] Y. Zhang, J. Xu, Y. Qu, X. Xi, J. Yang, *Ceram. Int.* **2014**, *40*, 5715.
[28] a) S. Lee, J. H. Choi, A. Park, M. Rim, J. Youn, W. Lee, J. E. Song, G. Khang, *Int. J. Biol. Macromol.* **2020**, *158*, 452; b) T.-R. Kim, M.-S. Kim, S. T. Goh, S. J. Lee, H. Y. Kim, S.-Y. Yoon, C.-S. Lee, *Appl. Sci.* **2019**, *9*, 1965.
[29] Q. T. Nguyen, Y. Hwang, A. C. Chen, S. Varghese, R. L. Sah, *Biomaterials* **2012**, *33*, 6682.
[30] a) W. C. Lee, C. H. Lim, C. S.u Kenry, K. P. Loh, C. T. Lim, *Small* **2015**, *11*, 963; b) J. Liao, Y. Qu, B. Chu, X. Zhang, Z. Qian, *Sci. Rep.* **2015**, *5*, 9879.
[31] H. Liang, Y. Bu, J. Zhang, *ACS Appl. Mater. Interfaces* **2013**, *5*, 6369.
[32] Y. Xin, T. Li, D. Gong, F. Xu, M. Wang, *RSC Adv.* **2017**, *7*, 6323.
[33] M. A. Bonifacio, P. Gentile, A. M. Ferreira, S. Cometa, E. De Giglio, *Carbohydr. Polym.* **2017**, *163*, 280.
[34] L. Vannozzi, I. C. Yasa, H. Ceylan, A. Menciassi, L. Ricotti, M. Sitti, *Macromol. Biosci.* **2018**, *18*, 1700377.
[35] D. Wu, Y. Yu, J. Tan, L. Huang, B. Luo, L. Lu, C. Zhou, *Mater. Des.* **2018**, *160*, 486.
[36] H. Yao, J. K. Xu, N. Y. Zheng, J. L. Wang, S. W. Mok, Y. W. Lee, L. Shi, J. Y. Wang, J. Yue, S. H. Yung, P. J. Hu, Y. C. Ruan, Y. F. Zhang, K. W. Ho, L. Qin, *Osteoarthritis Cartilage* **2019**, *27*, 1811.
[37] F. Ma, Y. Ge, N. Liu, X. Pang, X. Shen, B. Tang, *J. Mater. Chem. B* **2019**, *7*, 2463.
[38] Q. Chen, D. Wei, H. Chen, L. Zhu, C. Jiao, G. Liu, L. Huang, J. Yang, L. Wang, J. Zheng, *Macromolecules* **2015**, *48*, 8003.
[39] A. K. Means, C. S. Shrode, L. V. Whitney, D. A. Ehrhardt, M. A. Grunlan, *Biomacromolecules* **2019**, *20*, 2034.
[40] D. Kang, Z. Cai, Q. Jin, H. Zhang, *Carbon* **2015**, *91*, 445.
[41] a) S. Mun, H. C. Kim, M. Yadave, J. Kim, *Compos. Interfaces* **2015**, *22*, 249; b) S. M. Zargar, M. Mehdikhani, M. Rafienia, *J. Bioact. Compat. Polym.* **2019**, *34*, 331.
[42] D. C. Marcano, D. V. Kosynkin, J. M. Berlin, A. Sinitskii, Z. Sun, A. Slesarev, L. B. Alemany, W. Lu, J. M. Tour, *ACS Nano* **2010**, *4*, 4806.
[43] K. Sood, J. Kaur, H. Singh, S. Kumar Arya, M. Khatri, *Toxicol. Rep.* **2019**, *6*, 768.
[44] X. Zhou, M. Nowicki, H. Cui, W. Zhu, X. Fang, S. Miao, S.-J. Lee, M. Keidar, L. G. Zhang, *Carbon* **2017**, *116*, 615.
[45] J. Wang, J. Qiao, J. Wang, Y. Zhu, L. Jiang, *ACS Appl. Mater. Interfaces* **2015**, *7*, 9281.
[46] a) R. Balu, S. Reeder, R. Knott, J. Mata, L. de Campo, N. K. Dutta, N. R. Choudhury, *Langmuir* **2018**, *34*, 9238; b) Y. Meng, L. Ye, P. Coates, P. Twigg, *J. Phys. Chem. C* **2018**, *122*, 3157.

[47] a) C. Cha, S. R. Shin, X. Gao, N. Annabi, M. R. Dokmeci, X. Tang, A. Khademhosseini, *Small* **2014**, *10*, 514; b) R. Liu, S. Liang, X.-Z. Tang, D. Yan, X. Li, Z.-Z. Yu, *J. Mater. Chem.* **2012**, *22*, 14160.
[48] J. P. Gleghorn, L. J. Bonassar, *J. Biomech.* **2008**, *41*, 1910.
[49] Z. Wang, J. Li, L. Jiang, S. Xiao, Y. Liu, J. Luo, *Langmuir* **2019**, *35*, 11452.
[50] Z. Wang, J. Li, Y. Liu, J. Luo, *Tribol. Int.* **2020**, *143*, 106026.
[51] X. Gao, P. Ju, X. Liu, L. Chen, L. Ji, H. Li, H. Zhou, J. Chen, *Ind. Eng. Chem. Res.* **2019**, *58*, 5464.
[52] J. Tang, S. Chen, Y. Jia, Y. Ma, H. Xie, X. Quan, Q. Ding, *Carbon* **2020**, *156*, 272.
[53] Z. J. Zhang, D. Simionesie, C. Schaschke, *Lubricants* **2014**, *2*, 44.
[54] a) S. M. McNary, K. A. Athanasiou, A. H. Reddi, *Tissue Eng., Part B* **2011**, *18*, 88; b) P. E. Milner, M. Parkes, J. L. Puetzer, R. Chapman, M. M. Stevens, P. Cann, J. R. T. Jeffers, *Acta Biomater.* **2018**, *65*, 102; c) B. Wang, W. Tang, H. Lu, Z. Huang, *J. Mater. Chem. A* **2016**, *4*, 7257.
[55] L. V. Gibiansky, R. Lakes, *Mech. Mater.* **1997**, *25*, 79.
[56] F. Boschetti, G. Pennati, F. Gervaso, G. M. Peretti, G. Dubini, *Biorheology* **2004**, *41*, 159.
[57] G. Pattappa, B. Johnstone, J. Zellner, D. Docheva, P. Angele, *Int. J. Mol. Sci.* **2019**, *20*, 484.
[58] a) W. Zhao, X. Li, S. Gao, Y. Feng, J. Huang, *Cellulose* **2017**, *24*, 2095; b) J. Cui, M. A. Lackey, G. N. Tew, A. J. Crosby, *Macromolecules* **2012**, *45*, 6104; c) J. Hu, T. Kurokawa, K. Hiwatashi, T. Nakajima, Z. L. Wu, S. M. Liang, J. P. Gong, *Macromolecules* **2012**, *45*, 5218; d) C. W. Peak, J. J. Wilker, G. Schmidt, *Colloid Polym. Sci.* **2013**, *291*, 2031.
[59] D. K. Dempsey, C. Carranza, C. P. Chawla, P. Gray, J. H. Eoh, S. Cereceres, E. M. Cosgriff-Hernandez, *J. Biomed. Mater. Res., Part A* **2014**, *102*, 3649.
[60] L. Li, K. Zhang, T. Wang, P. Wang, B. Xue, Y. Cao, L. Zhu, Q. Jiang, *Mater. Des.* **2020**, *189*, 108492.
[61] S. Abdel-Jaber, C. Belvedere, A. Leardini, S. Affatato, *J. Biomech.* **2015**, *48*, 3830.
[62] A. J. S. Fox, A. Bedi, S. A. Rodeo, *Sports Health* **2012**, *4*, 340.
[63] K. J. Vazquez, J. T. Andreae, C. R. Henak, *J. Mech. Behav. Biomed. Mater.* **2019**, *98*, 262.
[64] C. Di Bella, S. Duchi, C. D. O'Connell, R. Blanchard, C. Augustine, Z. Yue, F. Thompson, C. Richards, S. Beirne, C. Onofrillo, S. H. Bauquier, S. D. Ryan, P. Pivonka, G. G. Wallace, P. F. Choong, *J. Tissue Eng. Regener. Med.* **2018**, *12*, 611.
[65] S. C. Shelmerdine, I. C. Simcock, J. C. Hutchinson, R. Aughwane, A. Melbourne, D. I. Nikitichev, J. L. Ong, A. Borghi, G. Cole, E. Kingham, A. D. Calder, C. Capelli, A. Akhtar, A. C. Cook, S. Schievano, A. David, S. Ourselin, N. J. Sebire, O. J. Arthurs, *Br. J. Radiol.* **2018**, *91*, 20180306.
[66] P. Kumar, A. Nagarajan, P. D. Uchil, *Cold Spring Harbor Protoc.* **2018**, *6*.
[67] W. Li, D. Wu, D. Hu, S. Zhu, C. Pan, Y. Jiao, L. Li, B. Luo, C. Zhou, L. Lu, *Mater. Sci. Eng., C* **2020**, *107*, 110333.
[68] C. Modrogan, A. M. Pandele, C. Bobirică, D. Dobrotă, A. M. Dăncilă, G. Gârleanu, O. D. Orbuleţ, C. Borda, D. Gârleanu, C. Orbeci, *Polymers* **2020**, *12*, 1182.
[69] O. Marciano, S. Gonen, N. Levy, E. Teblum, R. Yemini, G. D. Nessim, S. Ruthstein, L. Elbaz, *Langmuir* **2016**, *32*, 11672.
[70] Y. Gombert, R. Simič, F. Roncoroni, M. Dübner, T. Geue, N. D. Spencer, *Adv. Mater. Interfaces* **2019**, *6*, 1901320.
[71] A. Cafarelli, P. Losi, A. R. Salgarella, M. C. Barsotti, I. B. Di Cioccio, I. Foffa, L. Vannozzi, P. Pingue, G. Soldani, L. Ricotti, *J. Mech. Behav. Biomed. Mater.* **2019**, *97*, 138.
[72] A. Sharma, G. Desando, M. Petretta, S. Chawla, I. Bartolotti, C. Manferdini, F. Paolella, E. Gabusi, D. Trucco, S. Ghosh, G. Lisignoli, *ACS Biomater. Sci. Eng.* **2019**, *5*, 1518.